

Short WSRT HI observations of spiral galaxies*

M.-H. Rhee and T.S. van Albada

Kapteyn Astronomical Institute, Postbus 800, 9700 AV Groningen, The Netherlands
E-mail: rhee@astro.rug.nl and albada@astro.rug.nl

Received May 11; accepted August 29, 1995

Abstract. — We have obtained short HI observations of 60 late type spiral galaxies with the Westerbork Synthesis Radio Telescope (WSRT). Several HI properties are presented, including the radial surface density distribution of HI and a position-velocity map. When possible these are compared to those measured from single-dish observations. We confirm earlier results that there is no serious systematic difference between the WSRT and single-dish observations in total flux and linewidths.**

Key words: galaxies: fundamental parameters — galaxies: ISM — galaxies: kinematics and dynamics — galaxies: structure — galaxies: spiral — radio lines: galaxies

1. Introduction

We have observed 60 late type spiral galaxies with the Westerbork Synthesis Radio Telescope (WSRT; Högbom & Brouw 1974) in the 21-cm line of neutral hydrogen. The observations have been carried as so called *short observations* (see Sect. 2.2): the typical integration time is 2 hours per galaxy (for a full synthesis at least 12 hours is necessary). Such an observation contains essentially one-dimensional information along one particular direction (resolution axis), resulting in a position-velocity map. Short HI synthesis observations have several advantages over single-dish observations. From position-velocity maps several parameters can be measured, such as the maximum rotational velocity and HI isophotal diameters, in addition to the global parameters. Clearly, short observations do not contain the wealth of information of full 12-hour synthesis observations, e.g. no information on inclinations and position angles is available. But they are economic and adequate for our purpose: a study of the role of different definitions of 21-cm linewidths and rotational velocities on the Tully-Fisher relation (Tully-Fisher 1977) and of the systematics of the HI properties.

So far, statistical studies of the HI properties and the Tully-Fisher relation are mainly based on single-

dish measurements: the total number of galaxies with 2-dimensional HI velocity fields is still small. But the number of galaxies observed with the WSRT by means of short observations is now adequate for statistical analysis. In a separate paper, we will use our data and those of Broeils (1992) for studies of the Tully-Fisher relation and HI properties.

The selection criteria and general properties of the programme galaxies, observational method, data reduction, and analysis procedures are described in Sect. 2. In Sect. 3, several HI properties are presented and when possible compared to those measured from single-dish observations. A position-velocity map, a global profile and a strip integral for all 60 galaxies are presented in Sect. 3 as well.

2. Observations

2.1. Sample

In order to qualify for this project, a galaxy must have the following properties:

- (1) an angular diameter $D_{25} \geq 3'$, to make sure that we have sufficient independent data points to get a reasonable HI radial surface density profile and a rotation curve – assuming that the HI gas extends at least as far out as the optical disc.
- (2) an inclination $i \geq 40^\circ$ (as derived from optical data).
- (3) a declination $\delta > +15^\circ$, to make sure that a galaxy can be observed with the resolution axis along its optical major axis (see Sect. 2.2).
- (4) morphological type between Sab and Sd.

Send offprint requests to: M.-H. Rhee

*The Westerbork Synthesis Radio Telescope (WSRT) is operated by the Netherlands Foundation for Research in Astronomy (ASTRON) with financial support from the Netherlands Organization for Scientific Research (NWO)

**The tables also available in electronic form at CDS via ftp 130.79.128.5

Table 1. General properties of the sample galaxies

Name (1)	α h (2)	δ ° (3)	Type (4)	d Mpc (5)	i ° (6)	A_B^b mag (7)	A_B^i mag (8)	D_{25}^b ' (9)	$D_{25}^{b,i}$ kpc (10)	B_T mag (11)	$M_{B_T}^{b,i}$ mag (12)
NGC 7817	00 01 24.9	20 28 18	Sbc	32.9	81	0.27	0.96	3.55	27.1	12.41	-21.41
NGC 100	00 21 26.9	16 12 32	Sc	13.7	90	0.24	0.96	5.62	14.2	13.83	-18.05
NGC 514	01 21 24.8	12 39 22	SBc	34.3	35	0.23	0.32	3.63	36.4	12.26	-20.97
NGC 691	01 47 55.8	21 30 45	Sbc	37.3	45	0.27	0.37	3.39	36.3	12.26	-21.24
IC 167	01 48 22.2	21 40 01	SBc	40.8	50	0.27	0.40	2.75	31.5	13.60	-20.12
NGC 697	01 48 30.9	22 06 43	SBc	43.2	75	0.27	0.78	4.37	45.3	12.81	-21.42
NGC 772	01 56 35.3	18 45 50	Sb	34.6	58	0.27	0.47	7.41	69.9	10.94	-22.49
NGC 803	02 01 01.7	15 47 31	Sc	29.5	67	0.27	0.60	3.02	22.7	12.99	-20.23
NGC 918	02 23 03.7	18 16 20	SBc	21.9	56	0.30	0.44	3.47	20.9	13.07	-19.38
NGC 949	02 27 44.5	36 54 52	Sc	11.5	53	0.45	0.43	2.82	9.3	12.40	-18.77
NGC 1171	03 00 40.2	43 12 12	Sc	39.6	67	0.73	0.59	2.69	30.0	13.51	-20.79
IC 381	04 37 50.4	75 32 48	SBbc	37.8	57	0.67	0.46	2.57	28.7	13.12	-20.90
UGC 3137	04 39 18.8	76 19 36	Sbc	18.3	90	0.65	0.96	3.55	14.3	15.60	-17.33
NGC 2357	07 14 39.8	23 27 04	Sc	32.5	90	0.52	0.96	3.55	24.0	14.33	-19.71
NGC 2535	08 08 12.8	25 21 19	Sc	56.8	61	0.32	0.51	2.40	36.5	13.29	-21.31
NGC 2770	09 06 29.7	33 19 38	Sc	29.6	77	0.24	0.86	3.63	25.1	12.75	-20.70
IC 529	09 13 27.0	73 58 07	Sc	35.3	65	0.35	0.56	3.63	33.7	12.61	-21.04
NGC 3041	09 50 22.5	16 54 53	SBc	21.9	51	0.21	0.41	3.72	22.4	12.31	-20.01
UGC 5459	10 04 54.0	53 19 36	SBc	19.7	90	0.23	0.96	4.79	18.9	13.18	-19.48
NGC 3254	10 26 31.3	29 44 50	Sbc	22.4	78	0.20	0.87	4.79	25.1	12.40	-20.42
NGC 3264	10 29 08.6	56 20 27	SBcd	17.3	66	0.23	0.58	3.02	13.3	12.54	-19.46
NGC 3338	10 39 28.1	14 00 35	Sc	21.0	55	0.19	0.44	5.75	32.6	11.39	-20.84
NGC 3432	10 49 42.7	36 53 05	SBd	8.8	79	0.19	0.92	6.61	12.9	11.64	-19.19
NGC 3666	11 21 49.7	11 37 03	SBc	15.4	78	0.19	0.90	4.47	15.8	12.68	-19.35
NGC 3769	11 35 02.4	48 10 16	SBbc	13.0	77	0.21	0.85	2.75	8.4	12.52	-19.10
NGC 3949	11 51 05.2	48 08 16	Sc	14.6	55	0.21	0.44	2.88	11.5	11.49	-19.98
NGC 4100	12 03 36.4	49 51 36	Sc	19.6	76	0.21	0.82	5.37	24.7	11.85	-20.64
NGC 4144	12 07 28.3	46 44 07	Sbc	4.3	82	0.21	0.96	6.17	5.9	12.01	-17.31
NGC 4157	12 08 34.6	50 45 51	SBbc	14.2	90	0.21	0.96	6.61	19.4	12.10	-19.84
NGC 4183	12 10 47.2	43 58 35	Sc	15.0	90	0.20	0.96	5.25	15.1	12.83	-19.21
NGC 4217	12 13 21.7	47 22 12	Sab	18.9	85	0.21	0.96	4.90	21.6	12.04	-20.51
NGC 4414	12 23 58.2	31 30 05	Sc	8.7	56	0.19	0.44	3.80	8.9	10.92	-19.42
NGC 4534	12 31 38.8	35 47 41	Sc	11.3	38	0.19	0.34	2.88	9.4	13.04	-17.75
NGC 4545	12 32 20.3	63 48 10	SBc	41.7	57	0.26	0.45	2.51	28.5	13.16	-20.65
NGC 4814	12 53 13.3	58 37 07	Sb	38.9	47	0.24	0.38	3.31	36.5	12.77	-20.80
UGC 8146	13 00 03.6	58 58 19	Sc	13.3	90	0.24	0.96	3.47	8.6	14.58	-17.24
NGC 5023	13 09 58.0	44 18 13	Sc	6.4	90	0.21	0.96	6.03	7.4	12.82	-17.37
NGC 5205	13 28 19.1	62 46 10	Sbc	29.2	57	0.26	0.46	3.16	25.1	13.52	-19.53
NGC 5350	13 51 14.6	40 36 32	SBbc	36.1	39	0.19	0.34	3.24	33.6	12.22	-21.10
NGC 5351	13 51 18.9	38 09 36	SBbc	52.6	58	0.19	0.47	2.88	40.4	13.00	-21.26
NGC 5529	14 13 27.5	36 27 30	Sc	43.3	90	0.19	0.96	6.46	52.6	12.74	-21.60
NGC 5678	14 30 37.1	58 08 35	SBb	31.2	68	0.24	0.61	3.31	26.5	11.92	-21.40
NGC 5783	14 51 53.5	52 16 48	SBc	36.6	53	0.22	0.43	2.88	28.9	13.96	-19.50
NGC 5894	15 10 32.7	59 59 38	SBc	38.3	90	0.26	0.96	3.02	23.1	13.21	-20.93
NGC 5899	15 13 14.9	42 14 01	SBc	39.7	68	0.21	0.61	3.31	33.0	12.49	-21.33
NGC 5951	15 31 23.7	15 10 28	SBc	27.9	85	0.31	0.96	3.63	22.5	13.47	-20.03
NGC 6207	16 41 17.8	36 55 32	Sc	16.1	68	0.27	0.61	2.95	12.1	12.08	-19.84
NGC 6236	16 45 03.8	70 52 13	SBc	22.8	57	0.36	0.45	2.88	18.3	13.21	-19.40
NGC 6255	16 53 00.5	36 34 55	SBc	17.1	67	0.28	0.60	3.55	15.5	13.62	-18.42

Table 1. continued

Name	α h (1)	α m (2)	δ ° (3)	δ ' (4)	Type	d Mpc (5)	i ° (6)	A_B^b mag (7)	A_B^i mag (8)	D_{25} ' (9)	$D_{25}^{b,i}$ kpc (10)	B_T mag (11)	$M_{B_T}^{b,i}$ mag (12)		
NGC 6339	17	15	29.7	40	53	55	SBc	33.1	56	0.29	0.44	2.88	26.2	13.58	-19.75
NGC 6643	18	21	13.3	74	32	43	Sc	25.5	63	0.46	0.53	3.72	25.9	11.61	-21.41
NGC 6689	18	35	23.0	70	28	48	SBc	11.8	76	0.47	0.80	4.07	12.0	13.08	-18.56
UGC 11635	20	45	42.8	79	58	20	Sbc	68.8	69	0.61	0.63	2.88	54.0	14.35	-21.08
UGC 11651	20	55	05.5	25	46	27	Scd	24.0	78	0.90	0.89	3.16	19.9	15.16	-18.53
UGC 11707	21	12	20.2	26	31	37	Sc	15.9	59	0.75	0.48	3.55	16.7	15.35	-16.89
NGC 7177	21	58	18.5	17	29	50	SBb	18.3	51	0.41	0.41	3.16	16.8	11.92	-20.21
NGC 7497	23	06	34.9	17	54	20	SBc	25.2	72	0.30	0.70	4.27	26.6	12.94	-20.06
NGC 7664	23	24	10.6	24	48	18	Sc	48.7	58	0.32	0.46	2.63	35.1	13.41	-20.81
NGC 7741	23	41	22.7	25	47	53	SBC	13.3	47	0.31	0.38	4.47	16.9	11.72	-19.58
NGC 7753	23	44	33.2	29	12	22	SBbc	71.2	47	0.32	0.38	2.82	57.8	12.99	-21.97

Notes to Table 1

Column 1: Galaxy name

Columns 2 and 3: Right Ascension and Declination of the optical center (epoch 1950.0) (LEDA)

Column 4: Morphological type (LEDA)

Column 5: Distance to the galaxy (see text)

Column 6: Inclination (see text)

Columns 7 and 8: Galactic and internal extinctions in the B -band (see text)Column 9: Uncorrected blue major-axis isophotal diameter at the 25 mag/arcsec 2 (LEDA)

Column 10: Corrected blue major-axis isophotal diameter in kpc (see text)

Column 11: Uncorrected total apparent blue magnitude (LEDA)

Column 12: Corrected absolute blue magnitude ($= B_T - A_B^b - A_B^i - 5 \log d - 25$)

(5) no previous HI synthesis observations.

Galaxies meeting these criteria were selected from:

- (1) the list of Aaronson et al. (1982) with photometry in the H -band (~ 300 galaxies);
- (2) the master-list compiled by van Woerden for Broeils' survey (~ 300 galaxies; see Sect. 2.1 of Broeils & van Woerden 1994);
- (3) the list of Kent (1984, 1986) with surface photometry in the r -band (~ 150 galaxies).

Originally 105 galaxies were selected but later a number of galaxies with optical rotation curves from the list of Rubin et al. (1985) were added to the original list. About 60 galaxies have been observed with the WSRT. This sample, therefore, is not complete in any sense and some galaxies occasionally mildly violate the selection criteria. The general properties of the galaxies are listed in Table 1.

Most of the parameters in Table 1 are taken from the Lyon-Meudon Extragalactic Database (LEDA), which is constantly being updated. Note that the LEDA was used for constructing the RC3 (de Vaucouleurs et al. 1991). Information in Table 1 requiring explanation is as follows. The distance (Col. 5) to each galaxy has been calculated from the systemic velocity (Col. 2 of Table 5), corrected for the Virgo-centric flow following Kraan-Korteweg (1986), and a Hubble constant of 75

km s $^{-1}$ Mpc $^{-1}$. The inclination (Col. 6) has been calculated from the axial ratio (b/a) of the disc with the formula:

$$\cos^2 i = [(b/a)^2 - q_0^2]/(1 - q_0^2), \quad (1)$$

which treats a galaxy as an oblate spheroid ($i = 90^\circ$ corresponds to edge-on). Axial ratios ($b/a = d_{25}/D_{25}$) have been taken from LEDA. The parameter q_0 is the intrinsic flattening of the disc. To determine q_0 we use Fouqué et al.'s (1990) formula:

$$-\log q_0 = 0.43 + 0.053T \quad \text{for } -5 \leq T \leq 7, \quad (2)$$

where T is the morphological type code (RC3). The internal extinction (Col. 8) has been determined with the correction formula given by Tully & Fouqué (1985):

$$A_B^i = -2.5 \log[f(1 + e^{-\tau \sec i}) + (1 - 2f)(1 - e^{-\tau \sec i})]/(\tau \sec i), \quad (3)$$

where the optical depth $\tau = 0.55$ and $f = 0.25$. The corrected major axis isophotal diameter in kpc (Col. 10) at the 25 mag arcsec $^{-2}$ has been calculated following Tully & Fouqué (1985):

$$\log D_{25}^{b,i} = \log D_{25} - 0.22 \log(D_{25}/d_{25}) + 0.09 A_B^b + \log d + \log(0.2909), \quad (4)$$

Table 2. Observational parameters

Name (1)	Field Centre		Obs. date (4)	Obs. length (5)	Baseline		ϕ (8)	V_{obs} (9)	B (10)	ΔV (11)
	α h (2)	δ ° ' '' (3)			min (6)	max (7)				
NGC 7817	00 01 25	20 28 18	08 11 91	2.0	72	2736	44	2317	5.0	16.71
NGC 100	00 21 27	16 12 34	04 09 91	6.0	72	2736	56	840	2.5	8.28
NGC 514	01 21 25	12 39 22	01 11 91	2.0	54	2718	100	2477	2.5	8.37
NGC 691	01 47 56	21 30 45	08 10 91	2.0	72	2736	90	2660	5.0	16.75
IC 167	01 48 22	21 40 01	07 09 91	3.0	72	2736	85	2934	2.5	8.40
NGC 697	01 48 31	22 06 43	11 10 91	2.0	72	2736	105	3126	5.0	16.80
NGC 772	01 56 35	18 45 58	09 10 91	2.0	72	2736	131	2466	5.0	16.73
NGC 803	02 01 02	15 47 30	06 09 91	2.0	72	2736	137	2103	2.5	8.35
NGC 918	02 23 04	18 16 16	05 09 91	1.1	72	2736	155	1516	2.5	8.32
NGC 949	02 27 45	36 54 53	31 08 91	3.0	72	2736	142	610	2.5	8.27
NGC 1171	03 00 40	43 12 11	08 10 91	2.0	72	2736	148	2747	5.0	16.76
IC 381	04 37 50	75 32 44	13 10 91	1.9	72	2736	166	2485	5.0	16.73
UGC 3137	04 39 21	76 19 36	05 09 91	2.5	72	2736	75	944	2.5	8.29
NGC 2357	07 14 40	23 26 49	14 10 91	2.0	72	2736	123	2273	5.0	16.71
NGC 2535	08 08 13	25 21 19	05 09 91	1.0	72	2736	164	4100	2.5	8.46
NGC 2770	09 06 30	33 19 42	23 10 91	2.0	72	2736	149	1953	5.0	16.67
IC 529	09 13 28	73 58 06	04 11 91	2.0	54	2718	146	2261	5.0	16.71
NGC 3041	09 50 23	16 54 53	09 11 91	2.0	72	2736	86	1419	5.0	16.61
UGC 5459	10 04 54	53 19 45	07 11 91	2.0	72	2736	133	1121	5.0	16.58
NGC 3254	10 26 31	29 44 50	07 10 91	2.0	72	2736	47	1366	5.0	16.61
NGC 3264	10 29 08	56 20 30	06 09 91	1.0	72	2736	172	942	2.5	8.29
	10 29 08	56 20 30	04 09 91	1.5	72	2736	14	942	2.5	8.29
NGC 3338	10 39 28	14 00 34	04 11 91	2.0	54	2718	100	1301	5.0	16.60
NGC 3432	10 49 42	36 52 58	03 09 91	2.0	72	2736	39	613	2.5	8.27
NGC 3666	11 21 50	11 37 03	21 10 91	1.8	72	2736	100	1067	5.0	16.57
NGC 3769	11 35 02	48 10 16	09 11 91	2.0	72	2736	153	714	2.5	8.28
NGC 3949	11 51 05	48 08 16	08 11 91	2.2	72	2736	122	804	5.0	16.55
NGC 4100	12 03 36	49 51 36	08 11 91	2.0	72	2736	167	1076	5.0	16.58
NGC 4144	12 07 28	46 44 07	03 09 91	2.4	72	2736	106	265	2.5	8.25
NGC 4157	12 08 35	50 45 51	08 11 91	2.4	72	2736	66	771	5.0	16.54
NGC 4183	12 10 47	43 58 35	11 11 91	2.0	72	2736	166	933	2.5	8.29
NGC 4217	12 13 22	47 22 12	01 11 91	2.0	54	2718	50	1030	5.0	16.57
NGC 4414	12 23 58	31 29 54	23 10 91	1.9	72	2736	153	720	5.0	16.54
NGC 4534	12 31 39	35 47 41	11 11 91	2.2	72	2736	122	803	2.5	8.28
NGC 4545	12 32 20	63 48 01	01 11 91	1.0	54	2718	8	2723	5.0	16.76
NGC 4814	12 53 13	58 37 07	08 11 91	2.0	72	2736	109	2531	5.0	16.74
UGC 8146	13 00 03	58 58 06	03 09 91	2.1	72	2736	30	669	2.5	8.27
NGC 5023	13 09 58	44 18 13	04 09 91	2.2	72	2736	30	400	2.5	8.26
NGC 5205	13 28 19	62 46 12	05 09 91	1.3	72	2736	169	1781	2.5	8.34
	13 28 19	62 46 12	03 09 91	1.1	72	2736	10	1781	2.5	8.34
NGC 5350	13 51 15	40 36 35	07 10 91	2.0	72	2736	47	2316	5.0	16.71
NGC 5351	13 51 19	38 09 36	09 11 91	2.0	72	2736	99	3620	5.0	16.86
NGC 5529	14 13 28	36 27 30	21 10 91	2.0	72	2736	115	2880	5.0	16.77
NGC 5678	14 30 37	58 08 35	07 11 91	1.0	72	2736	171	1931	5.0	16.67
	14 30 37	58 08 35	08 10 91	1.0	72	2736	9	1931	5.0	16.67
NGC 5783	14 51 54	52 16 48	05 09 91	1.0	72	2736	171	2330	2.5	8.36
	14 51 54	52 16 48	01 11 91	1.2	54	2718	13	2330	2.5	8.36
NGC 5894	15 10 32	59 59 42	07 10 91	2.0	72	2736	17	2485	5.0	16.73

Table 2. continued

Name	Field Centre			Obs. date	Obs. length	Baseline		ϕ	V_{obs}	B	ΔV	
	α h	m	s	δ °	'	"	min m	max m	°	km/s	MHz	km/s
(1)	(2)	(3)		(4)	(5)		(6)	(7)	(8)	(9)	(10)	(11)
NGC 5899	15 13 15	42 14 01		11 10 91	2.0	72	2736	22	2580	5.0	16.74	
NGC 5951	15 31 24	15 10 27		03 09 91	1.0	72	2736	28	1784	2.5	8.34	
NGC 6207	16 41 18	36 55 32		11 11 91	1.0	72	2736	168	852	2.5	8.28	
	16 41 18	36 55 32		03 09 91	1.1	72	2736	14	852	2.5	8.28	
NGC 6236	16 45 04	70 52 13		04 09 91	2.0	72	2736	15	1288	2.5	8.31	
NGC 6255	16 53 01	36 34 51		05 09 91	2.3	72	2736	85	921	2.5	8.29	
NGC 6339	17 15 30	40 53 52		05 09 91	1.0	72	2736	11	2111	2.5	8.35	
NGC 6643	18 21 13	74 32 40		12 10 91	2.0	72	2736	38	1490	5.0	16.62	
NGC 6689	18 35 22	70 28 57		03 09 91	1.0	72	2736	171	487	2.5	8.26	
	18 35 22	70 28 57		31 08 91	1.2	72	2736	9	487	2.5	8.26	
UGC 11635	20 45 43	79 58 20		09 10 91	2.0	72	2736	35	4799	5.0	16.99	
UGC 11651	20 55 05	25 46 29		13 10 91	1.0	72	2736	18	1527	5.0	16.62	
UGC 11707	21 12 20	26 31 39		01 09 91	3.0	72	2736	52	908	2.5	8.29	
NGC 7177	21 58 19	17 29 50		15 10 91	2.0	72	2736	82	1188	5.0	16.59	
NGC 7497	23 06 35	17 54 23		16 10 91	2.0	72	2736	48	1716	5.0	16.65	
NGC 7664	23 24 11	24 48 18		12 10 91	2.0	72	2736	87	3464	5.0	16.84	
NGC 7741	23 41 23	25 47 53		07 09 91	1.0	72	2736	18	750	2.5	8.28	
NGC 7753	23 44 33	29 12 22		11 10 91	2.0	72	2736	64	5163	5.0	17.03	

Notes to Table 2

Column 1: Galaxy name

Columns 2 and 3: Right Ascension and Declination of the field center (epoch 1950.0)

Column 4: Date of observation

Column 5: Duration of observation

Columns 6 and 7: Minimum and maximum baselines

Column 8: Position angle of the resolution axis

Column 9: Radial velocity of the central channel

Column 10: Bandwidth of the observation

Column 11: Velocity spacing of the channels (the velocity resolution is twice this value)

where D_{25}/d_{25} is the major-to-minor axis ratio at the 25 mag/arcsec $^{-2}$ blue isophotal level taken from LEDA and d the distance to the galaxy as listed in Table 1.

2.2. Short observations

Since the techniques of short WSRT observations have been described many times before, we will only briefly discuss them; for details see Warmels (1986, 1988a), Oosterloo (1988), Oosterloo & Shostak (1993), Broeils (1992) and Broeils & van Woerden (1994).

Because the (u,v) -plane coverage of observations of a few hours (typically two) is limited, a short WSRT observation contains essentially one-dimensional information along a particular direction: the resolution axis. Along the resolution axis, the half power beam width (HPBW) of a short observation is about the same as that of a full synthesis observation. At the wavelength of 21-cm, the

HPBW on the resolution axis, θ , is given by the formula:

$$\theta = 12'' \cdot (\cos^2 h + \sin^2 h \sin^2 \delta)^{-1/2}, \quad (5)$$

where h is the average hour angle of the observation and δ the declination of the pointing centre. In the direction perpendicular to the resolution axis, the HPBW is in general at least several arcminutes: in this direction galaxies are essentially unresolved. To obtain information such as HI diameter and maximum rotational velocity, it is important to perform the observation in such a way that the resolution axis matches the major axis of the galaxy. The position angle, ϕ , of the resolution axis can be determined from:

$$\cot(\phi + \pi) = \tan h \sin \delta \quad \text{for } 0^\circ \leq \phi < 180^\circ, \quad (6)$$

where ϕ is measured from north eastward. Scheduling of the observations was done with Eq. (6), using the optical position angle of the major axis for ϕ . The observational parameters are summarized in Table 2.

Table 3. Parameters of the position-velocity maps

Name (1)	l ' (2)	ϕ ° (3)	θ '' (4)	σ $\frac{\text{mJy}}{\text{beam}}$ (5)	Name (1)	l ' (2)	ϕ ° (3)	θ '' (4)	σ $\frac{\text{mJy}}{\text{beam}}$ (5)
NGC 7817	3	44	35	3.0	NGC 4217	4	50	19	2.8
NGC 100	5	56	38	3.7	NGC 4414	4	153	32	3.1
NGC 514	9	100	22	3.3	NGC 4534	4	122	22	3.1
NGC 691	5	90	15	2.7	NGC 4545	6	8	20	4.0
IC 167	4	85	19	2.7	NGC 4814	4	109	19	3.9
NGC 697	5	105	20	2.4	UGC 8146	6	30	20	4.4
NGC 772	3	131	35	3.2	NGC 5023	4	30	25	4.1
NGC 803	2	137	37	3.5	NGC 5205	5	10	21	5.2
NGC 918	3	155	44	4.4	NGC 5350	8	47	26	4.6
NGC 949	4	142	28	3.5	NGC 5351	3	99	16	2.4
NGC 1171	5	148	27	3.6	NGC 5529	4	115	19	3.0
IC 381	4	166	19	4.0	NGC 5678	6	10	24	3.7
UGC 3137	8	75	19	7.1	NGC 5783	4	172	24	4.1
NGC 2357	4	123	28	3.2	NGC 5894	5	17	24	3.5
NGC 2535	4	164	36	6.0	NGC 5899	4	22	27	3.0
NGC 2770	3	149	29	3.0	NGC 5951	2	28	47	4.8
IC 529	4	146	19	3.0	NGC 6207	4	15	30	4.4
NGC 3041	10	86	18	2.9	NGC 6236	5	15	20	4.5
UGC 5459	2	133	17	2.7	NGC 6255	3	85	17	2.9
NGC 3254	3	47	25	2.7	NGC 6339	5	11	26	5.6
NGC 3264	5	172	20	5.4	NGC 6643	10	38	25	5.4
NGC 3338	8	100	21	2.8	NGC 6689	5	171	20	5.0
NGC 3432	4	39	21	4.6	UGC 11635	4	35	19	1.9
NGC 3666	9	100	21	2.7	UGC 11651	7	18	40	4.9
NGC 3769	7	153	28	5.0	UGC 11707	10	52	35	5.6
NGC 3949	11	122	26	4.5	NGC 7177	5	82	16	2.7
NGC 4100	7	167	28	3.8	NGC 7497	4	48	37	3.9
NGC 4144	3	106	18	3.3	NGC 7664	7	87	18	2.5
NGC 4157	6	66	20	3.1	NGC 7741	7	18	40	6.3
NGC 4183	4	166	27	3.7	NGC 7753	6	64	25	2.7

Notes to Table 3

Column 1: Galaxy name

Column 2: Integration length perpendicular to the resolution axis

Column 3: Position angle of the resolution axis

Column 4: Half power beam width of the integrated antenna pattern

Column 5: Noise level in the position-velocity map

The calibration was done by observing a standard WSRT calibration source before and after each observation, following the procedures described by van Someren Greve (1971).

2.3. Data reduction

Fourier transformations were calculated with the LINE-JOB package, resulting in data cubes of 63 channel maps. The remaining data reduction has been done with the Groningen Image Processing SYstem (GIPSY; Allen et al. 1985). We used essentially the same method as that of Warmels (1986, 1988a), Oosterloo (1988), Oosterloo &

Shostak (1993), Broeils (1992) and Broeils & van Woerden (1994).

First, the channel maps were rotated in such a way that they had the resolution axis in the horizontal and the unresolved axis in the vertical direction; then they were integrated over the unresolved direction with different integration lengths, resulting in a series of position-velocity maps with position along the resolution axis and heliocentric velocity as coordinates. Ideally, the integration length should correspond to the size of the true HI distribution convolved with the synthesized beam. However, as this quantity is not known a priori, we determined the optimum integration length empirically by selecting

Table 4. HI fluxes, masses, diameters and effective surface densities

Name (1)	F_{HI} Jy km s (2)	M_{HI} $10^9 M_{\odot}$ (3)	D_{HI} kpc (4)	R_{eff} kpc (5)	μ_{eff} M_{\odot} pc 2 (6)	Name (1)	F_{HI} Jy km s (2)	M_{HI} $10^9 M_{\odot}$ (3)	D_{HI} kpc (4)	R_{eff} kpc (5)	μ_{eff} M_{\odot} pc 2 (6)
NGC 7817	17	4.40	34	13	2.9	NGC 4217	26	2.15	27	9	4.8
NGC 100	47	2.05	33	11	2.7	NGC 4414	63	1.14	20	6	3.2
NGC 514	26	7.20	47	14	6.3	NGC 4534	62	1.87	25	7	5.1
NGC 691	13	4.37	43	15	4.5	NGC 4545	14	5.77	44	12	5.6
IC 167	23	9.18	55	17	5.9	NGC 4814	23	8.09	57	16	4.1
NGC 697	48	21.18	76	21	6.7	UGC 8146	32	1.32	21	6	4.6
NGC 772	90	25.46	91	31	3.0	NGC 5023	56	0.53	15	4	4.3
NGC 803	30	6.16	41	11	7.2	NGC 5205	16	3.13	32	12	4.6
NGC 918	23	2.56	32	9	5.1	NGC 5350	30	9.17	67	16	3.8
NGC 949	19	0.60	15	5	2.5	NGC 5351	20	12.82	61	17	4.9
NGC 1171	22	8.16	58	16	2.6	NGC 5529	36	15.90	83	25	3.6
IC 381	24	8.08	56	13	3.9	NGC 5678	16	3.72	28	7	10.4
UGC 3137	36	2.85	26	8	4.6	NGC 5783	20	6.39	46	14	5.6
NGC 2357	35	4.15	53	15	5.8	NGC 5894	12	4.18	26	10	5.3
NGC 2535	20	14.90	74	24	4.4	NGC 5899	16	5.98	44	15	3.1
NGC 2770	34	7.04	42	11	7.1	NGC 5951	20	3.66	32	8	7.6
IC 529	27	7.93	48	14	5.6	NGC 6207	31	1.90	23	6	6.6
NGC 3041	22	2.52	35	9	4.4	NGC 6236	21	2.53	24	7	7.6
UGC 5459	47	4.30	39	11	5.4	NGC 6255	24	1.67	22	7	7.9
NGC 3254	44	5.23	42	13	5.5	NGC 6339	12	3.18	33	10	4.5
NGC 3264	20	1.40	20	6	6.0	NGC 6643	32	4.91	31	9	12.3
NGC 3338	116	12.02	63	18	3.9	NGC 6689	35	1.14	20	6	3.6
NGC 3432	100	1.81	25	8	2.5	UGC 11635	13	14.59	73	24	4.6
NGC 3666	48	2.69	30	8	4.5	UGC 11651	19	2.61	31	9	5.5
NGC 3769	40	1.57	20	6	5.1	UGC 11707	59	3.54	32	9	6.0
NGC 3949	39	1.98	18	5	14.4	NGC 7177	21	1.63	22	6	4.7
NGC 4100	40	3.65	40	13	3.3	NGC 7497	64	9.49	52	14	7.7
NGC 4144	51	0.22	8	2	5.1	NGC 7664	27	15.13	69	20	3.4
NGC 4157	78	3.72	36	9	5.3	NGC 7741	52	2.13	23	5	12.3
NGC 4183	46	2.46	31	9	4.6	NGC 7753	23	27.96	105	34	2.9

Notes to Table 4

Column 1: Galaxy name

Column 2: Total HI flux integral

Column 3: Total HI mass

Column 4: HI isophotal diameter at the level of $1 M_{\odot}/\text{pc}^2$

Column 5: HI effective radius, enclosing 50% of the HI mass

Column 6: HI surface density at the HI effective radius

the position-velocity map with the highest signal-to-noise ratio. The optimum integration lengths are listed in Table 3. Subtraction of continuum was done on the position-velocity map: the continuum emission was determined by a least-squares fit to the points in the line-free velocity channels and then removed from the position-velocity map. The antenna pattern was integrated in the same way as the channel maps and normalized to its central peak value. Due to the limited u, v coverage, the resulting antenna pattern has a non-Gaussian shape and suffers from large side-lobes with negative values up to 30 – 40% of the central peak, resulting in large depressions in the position-velocity

map. In order to remove these instrumental effects, we have CLEANed (Högbom 1974) the position-velocity map with the corresponding antenna pattern. The HPBW of the integrated antenna pattern and the rms noise levels in the cleaned position-velocity map are tabulated in Table 3. The cleaned position-velocity maps have further been corrected for primary beam attenuation. The resulting position-velocity maps are presented in Fig. 4.

3. HI properties

3.1. Total HI fluxes and masses

We have determined the total HI flux of a galaxy by adding the flux of all CLEAN components to the residuals and by correcting for the primary beam attenuation. The HI mass can be determined in units of solar mass (M_{\odot}) from the standard formula given below, assuming that the HI gas is optically thin:

$$M_{\text{HI}} = 2.36 \cdot 10^5 d^2 FI \quad (M_{\odot}), \quad (7)$$

where FI is the total HI flux integral in units of Jy km/s and d is the distance to the galaxy in Mpc. The total HI fluxes and masses are listed in Table 4.

The uncertainty in the determination of the HI flux density depends on several parameters: the calibration quality, the continuum subtraction, the integration area, and the rms noise in the position-velocity map. From a comparison of the HI flux densities of the same galaxy, observed twice at different position angles (see Table 2), we estimate that the combined uncertainty is of order 10 – 15% (see also Broeils & van Woerden 1994).

It is well known that the flux of an extended source measured with a synthesis telescope is often underestimated due to the missing zero spacing. For instance, because the shortest spacing in our WSRT observations is either 54 or 72 m, the observations are insensitive to structures larger than 7 and 5 arcmin, respectively. On the other hand, fluxes measured with single-dish telescopes often need to be corrected for the effects of source extent when the (unknown) HI angular diameter of galaxy is larger than the beam size. The correction for this source-to-beam ratio (the so called beam-filling correction) can be substantial, depending on the true HI gas distribution and on the telescope and feed used for the observation. To estimate the beam-filling correction factor, in general, the HI surface density distribution is represented by some analytical function in which the HI scale length is taken as a fixed fraction of the optical radius (see Haynes & Giovanelli 1984; Bottinelli et al. 1990). Bottinelli et al. (1990), for instance, adopt a beam-filling correction factor expressed by the formula:

$$R = (1 + (pD_{25}/\alpha)^2)^{1/2} (1 + (pd_{25}/\alpha)^2)^{1/2}, \quad (8)$$

where R is the ratio of the corrected flux to the raw one, p is a constant depending on the adopted diameter system (e.g. D_{25} or Holmberg radius) and α is the half power beam size of the radio telescope. In view of this, comparison of the fluxes measured with synthesis and single-dish telescopes is not straightforward. In Fig. 1a, total HI fluxes from 11 different telescopes and 33 publications listed in the HI catalogue by Huchtmeier & Richter (1989) are plotted against our WSRT fluxes. In spite of the inhomogeneous nature of the single-dish data (different instruments, different reduction and correction methods, etc.),

the general agreement between the WSRT and single-dish HI fluxes is quite good. Note that Huchtmeier & Richter's (1989) catalogue contains data as originally published. We have made a least-squares fit to the data points in Fig. 1a to compare the two flux scales quantitatively, adopting the bisector of the direct and inverse least-squares fits as the representative fit. Removing 4 extreme outliers seen in Fig. 1a, we find:

$$\log FI_{\text{SD}} = 1.07 (\pm 0.03) \log FI_{\text{WSRT}} - 0.12 (\pm 0.04), \quad (9)$$

where FI_{SD} and FI_{WSRT} are the single-dish and the WSRT total HI fluxes in units of Jy km/s on a logarithmic scale, respectively. The standard deviation with respect to the fitted line is 0.08 dex. Since the LEDA lists homogenized mean HI fluxes (i.e. averaged and corrected for various effects according to Bottinelli et al. 1990), we expect smaller scatter if we use the LEDA HI fluxes instead of the inhomogeneous ones taken from Huchtmeier & Richter's catalogue (1989) in the comparison. With LEDA the comparison of the HI fluxes is indeed more favourable, as seen in Fig. 1b. From the least-squares fit to the data points in Fig. 1b, given by:

$$\log FI_{\text{LEDA}} = 1.04 (\pm 0.03) \log FI_{\text{WSRT}} + 0.02 (\pm 0.04), \quad (10)$$

we find that the standard deviation with respect to the fitted line is 0.05 dex. FI_{LEDA} and FI_{WSRT} represent the total HI fluxes from the LEDA and WSRT in units of Jy km/s, respectively. The results of the least-squares fits of the data points in Fig. 1 indicate that there exists no serious systematic effect between the HI flux scale of the WSRT and that of single-dish observations, at least in our sample of galaxies, confirming Broeils' results (1992; see also Broeils & van Woerden 1994). The mean HI flux differences are also small: $\langle FI_{\text{WSRT}} - FI_{\text{SD}} \rangle = 0 \pm 9$ and $\langle FI_{\text{WSRT}} - FI_{\text{LEDA}} \rangle = -3 \pm 6$ Jy km/s.

In the earlier study of spiral galaxies in the Virgo cluster, Warmels (1986, 1988a) found a small ($\approx 12\%$) systematic difference between FI_{WSRT} and FI_{SD} , and suspected that some of the flux was missed by the WSRT (due to the lack of spacings shorter than 72 m) or that systematic errors in the reduction procedures were present. Broeils (1992; see also Broeils & van Woerden 1994), basing himself on diameter size arguments, concluded that missing flux in the observations by Warmels is unlikely to be the main cause of the systematic HI flux difference between the WSRT and single-dish measurements. Coming back to Warmels' second possibility, i.e. systematic errors in the reduction procedures, it is important to note that the average value of the HI-to-optical diameter ratio ($D_{\text{HI}}/D_{25}^{b,i}$) for the field galaxies is larger than that for galaxies in the Virgo cluster (Warmels 1986). Furthermore, this value shows a trend with the projected angular distance from the Virgo cluster center. Therefore, the beam-filling correction factors for the single-dish fluxes of the Virgo cluster galaxies may have been overestimated. New modeling

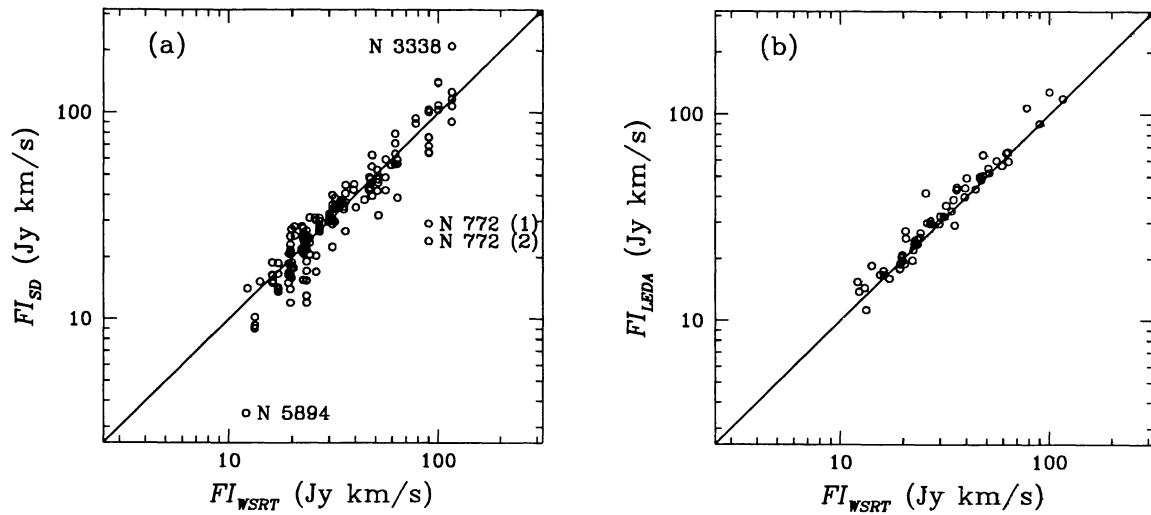


Fig. 1. a) The single-dish total HI fluxes taken from various sources (tabulated in Huchtmeier & Richter (1989)) are plotted against the WSRT total HI fluxes determined in this study. Four extreme outliers are marked with NGC numbers. The total HI flux of NGC 5894 has been taken from Wootten et al.'s private contribution (Huchtmeier & Richter 1989). The deviating value of the HI flux of NGC 3338 has been taken from Kreitschmann's unpublished Ph.D. thesis (1985) from the University of Bochum (Huchtmeier & Richter 1989). Therefore it is not possible to investigate what causes the discrepancy in total flux for these two galaxies. The two small HI fluxes of NGC 772 have been obtained with the Arecibo 305 m telescope (Davis & Seaquist 1983 for (1) and Dickel & Rood 1980 for (2)), and have not been corrected for beam-filling. Therefore, the main cause of the flux discrepancy in NGC 772 is undersampling of the HI gas due to the small beam size (HPBW of 3.8 arcmin) of the Arecibo telescope compared to the HI size of NGC 772 ($D_{HI} = 9.0$ arcmin). b) The total HI fluxes taken from LEDA are plotted against our measurements. For this comparison, the HI line magnitudes, m_{21} , listed in LEDA have been transformed to the $FI_{LED A}$ expressed in units of Jy km/s through the relation described in the RC3: $\log FI_{LED A} = 0.4(16.6 - m_{21}) + 0.3244 + \log(1 + z)$ where z is the redshift of the galaxy. The solid lines indicate equal results

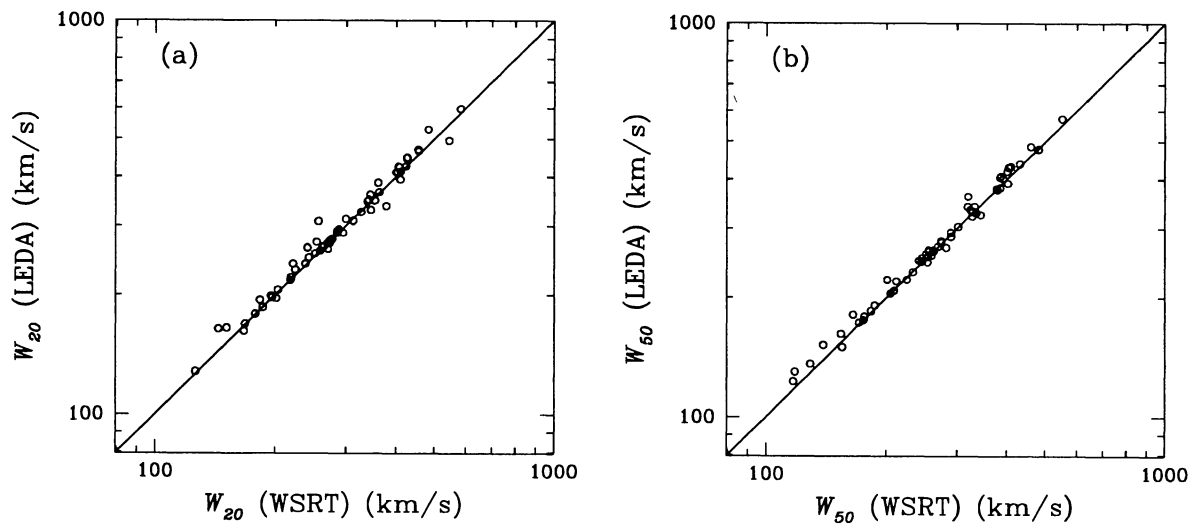


Fig. 2. a) The 20% HI linewidths taken from LEDA are plotted against our values measured at 20% of the peak flux of the profile (first method). b) Same as a) but for the 50% HI linewidths. The solid lines indicate equal results

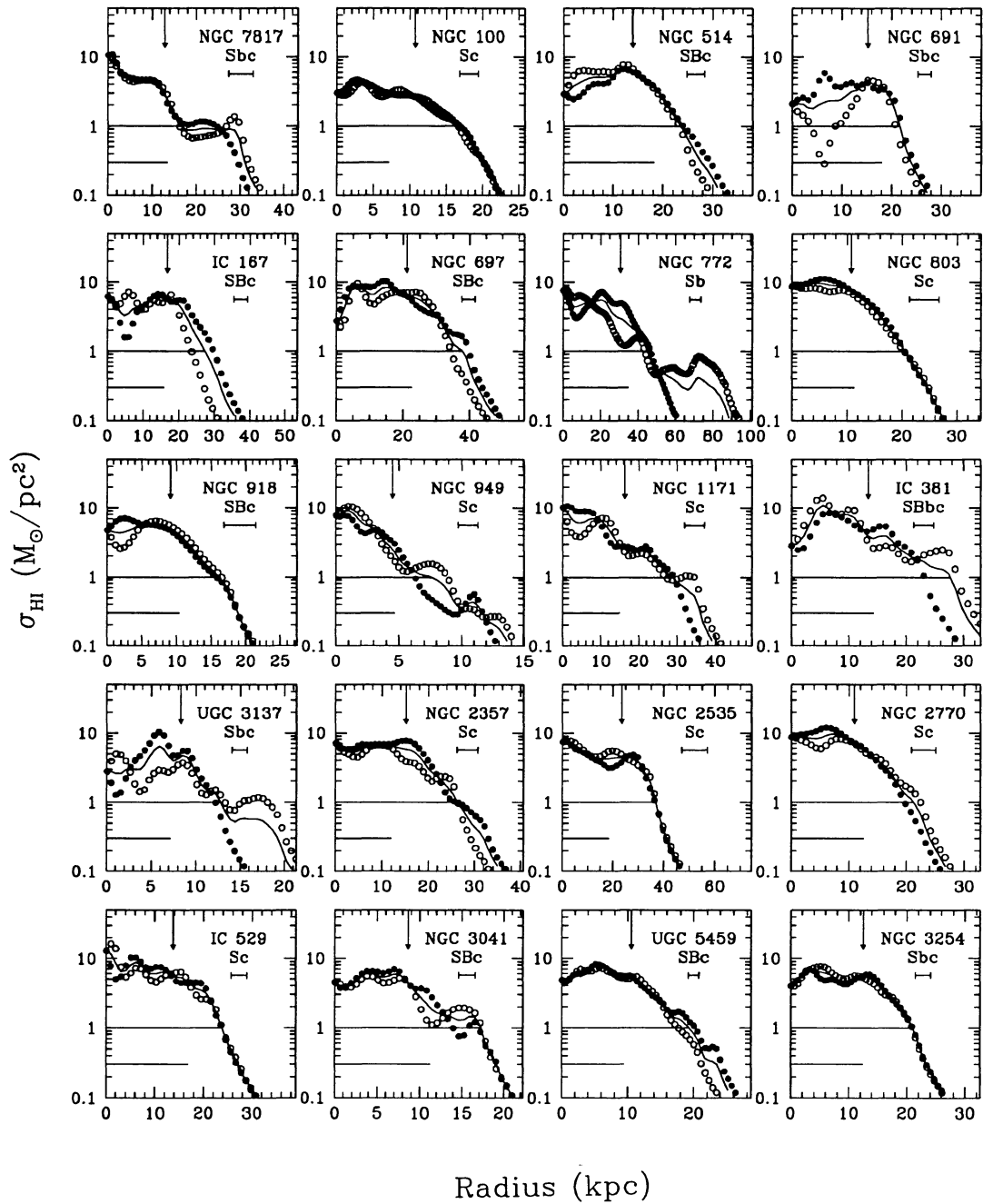


Fig. 3. HI surface density profiles. Open and filled circles represent approaching and receding sides of the galaxy, respectively: the average values are shown with the solid lines. The top and bottom horizontal lines indicate the HI ($D_{\text{HI}}/2$) and the optical ($D_{25}/2$) radii, respectively. The arrows point at the effective HI radius (R_{eff}). The error bars indicate the HPBW of the integrated antenna pattern in kpc

based on a large sample of synthesis observation data is needed to verify this point.

3.2. Systemic velocities and HI line profile widths

Several methods for determining HI linewidths at different levels of HI signal intensity are found in the literature (see e.g. Huchtmeier & Richter 1989). Since no ideal method

appears to exist, we have determined the HI linewidth with four different methods: three widely applied in the literature and one proposed in this paper.

The HI profile linewidths are defined as the radial velocity differences between the high and low velocity edges, measured at the signal levels equal to 20 and 50% of

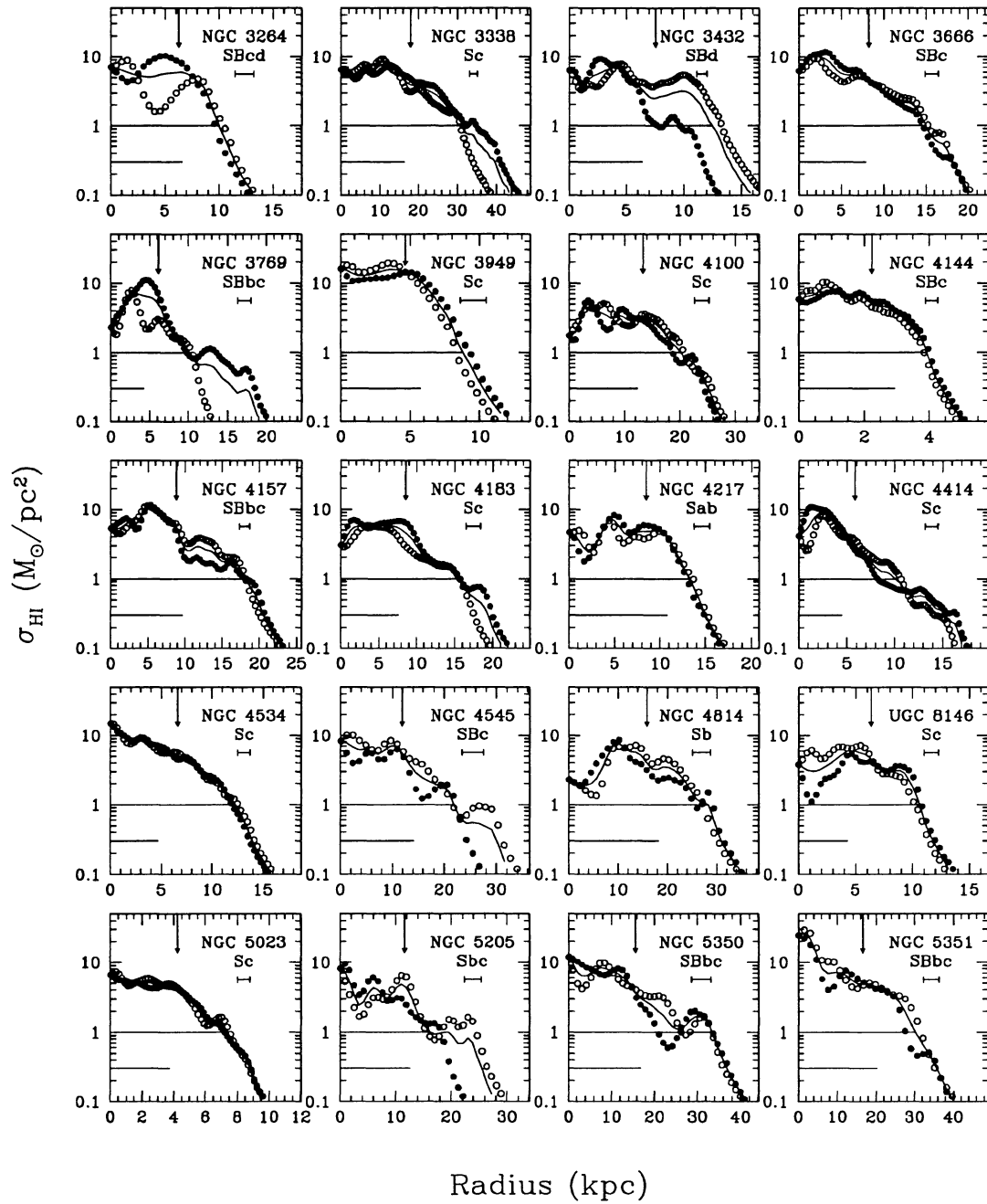


Fig. 3. continued

- (1) the peak flux of the profile (e.g. Tully 1988; Bottinelli et al. 1990; LEDA);
- (2) the peak fluxes in each half of the profile, separately;
- (3) the average of the peak fluxes in the two halves of the profile (e.g. Sullivan et al. 1981; Bothun et al. 1985);
- (4) the mean flux of the profile (e.g. Haynes & Giovanelli 1984; Bicay & Giovanelli 1986).

Richter & Sancisi (1994) concluded, after careful analysis of more than 1700 HI spectra, that lopsided HI distributions and kinematics usually result in an asymmetry

of the global HI profile, and asymmetries in disc galaxies may be the rule rather than the exception. The proposal of the second method is motivated by their work: explicitly taking into account asymmetry would imply that use of the two peak fluxes separately is superior to the use of an average. The systematic velocities at the 20 and 50% level can then be determined by averaging two edge velocities. The final systemic velocity has been determined from the error-weighted mean of the 20 and 50% level systemic velocities. The errors in the linewidths have been estimated

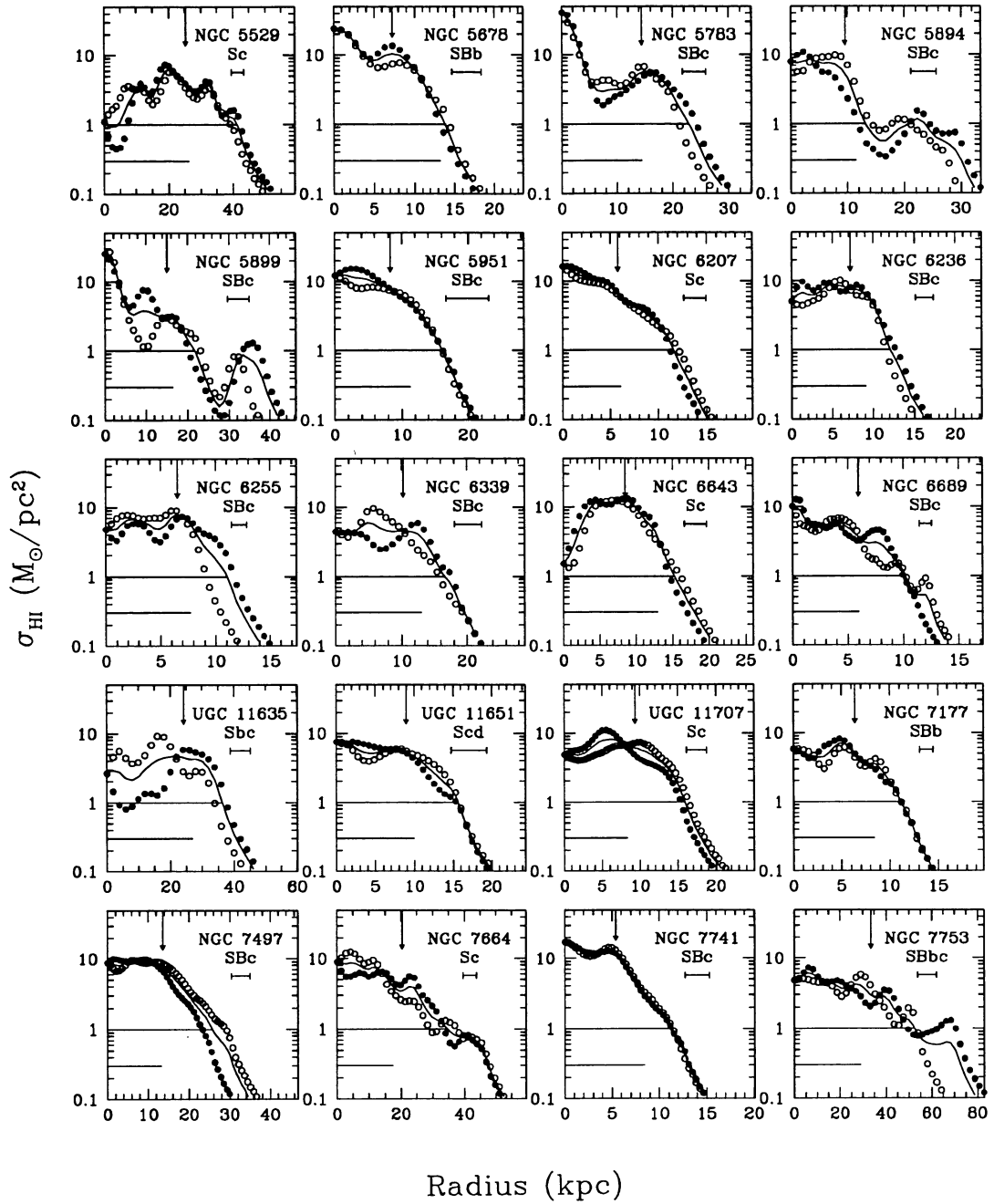


Fig. 3. continued

by allowing the edge-velocity in each case to vary by the rms noise in the global profile and then re-calculating the linewidth (Sullivan et al. 1981; see also Broeils 1992): the errors, therefore, are internal. The systemic velocities and linewidths from the four different methods, and their errors, are listed in Table 5. The 20% linewidth determined with the fourth method is not favoured because of its great sensitivity to the noise in the profile. It is not possible to choose among the other methods on the basis of their internal mean errors, which are similar.

It has been suggested that for the Virgo cluster galaxies the HI linewidths measured with the WSRT are systematically larger than those measured with single-dish telescopes (Pierce & Tully 1988; Fouqué et al. 1990). Broeils & van Woerden (1994) suspected that this systematic difference might be due to insufficient correction of the WSRT linewidths for instrumental broadening. Recently, Verheijen (private communication) indeed confirmed that this was the case: when the same correction method for

Table 5. Systemic velocities and HI linewidths

Name (1)	V_{sys}^1 (2)	W_{20}^1 (3)	W_{50}^1 (4)	V_{sys}^2 (5)	W_{20}^2 (6)	W_{50}^2 (7)	V_{sys}^3 (8)	W_{20}^3 (9)	W_{50}^3 (10)	V_{sys}^4 (11)	W_{20}^4 (12)	W_{50}^4 (13)
		$W_{20}^{1,c}$ (14)	$W_{50}^{1,c}$ (15)		$W_{20}^{2,c}$ (16)	$W_{50}^{2,c}$ (17)		$W_{20}^{3,c}$ (18)	$W_{50}^{3,c}$ (19)			
NGC 7817	2306± 7	426±25	389± 10	2306± 7	427±26	390±10	2306± 7	427±26	390±10	2310± 9	450±19	419±19
	408	385	408		408	385		409	385			
NGC 100	841± 1	228± 3	211± 2	840± 1	229± 3	212± 2	841± 1	228± 3	212± 2	841± 2	238± 8	224± 3
	219	209	219		219	210		219	210			
NGC 514	2472± 3	262± 9	247± 5	2471± 3	263±10	248± 5	2471± 3	263± 9	248± 5	2470± 3	269± 5	259± 6
	253	245	253		246	253		253	246			
NGC 691	2669± 7	364±14	332±12	2666± 8	371±16	341±15	2669± 8	369±15	339±17	2667± 8	382±18	359±13
	346	328	352		336	351		335				
IC 167	2931± 2	188± 7	142± 2	2928± 2	190± 7	148± 2	2931± 2	192± 8	147± 2	2931± 3	222±19	184± 4
	178	139	181		146	182		144				
NGC 697	3117± 5	475±11	436±10	3114± 5	479±11	445± 9	3116± 5	478±11	442± 9	3113± 5	490±11	464±10
	456	432	460		440	459		438				
NGC 772	2478± 6	473± 9	410±16	2473± 5	478±11	427± 8	2477± 5	478±10	424± 9	2475± 6	502±16	465± 9
	455	405	460		423	460		420				
NGC 803	2101± 1	273± 3	255± 2	2100± 1	275± 4	258± 2	2101± 1	275± 4	258± 2	2101± 2	285± 9	271± 3
	264	253	266		256	266		266	256			
NGC 918	1507± 3	271± 5	248± 6	1508± 3	272± 5	251± 5	1507± 3	272± 6	250± 6	1507± 3	279± 5	264± 5
	262	245	263		248	263		248				
NGC 949	609± 2	211± 6	177± 3	608± 2	211± 6	178± 3	609± 2	211± 6	178± 3	611± 2	221± 5	194± 4
	201	175	202		176	202		176				
NGC 1171	2740± 6	314±12	286±11	2740± 6	314±12	287±11	2740± 6	314±12	287±11	2740±11	332±16	308±40
	295	282	295		282	295		282				
IC 381	2476± 3	304± 6	273± 6	2477± 3	304± 6	275± 6	2476± 3	304± 6	275± 6	2476± 4	311±11	291± 6
	285	269	286		271	286		271				
UGC 3137	990± 5	230±10	203±10	990± 5	230±10	203±10	990± 5	230±10	203±10	992± 5	235± 9	215± 9
	221	201	221		201	221		221	201			
NGC 2357	2269± 3	363± 6	328± 6	2267± 3	367± 6	335± 5	2269± 3	366± 6	334± 5	2268± 4	376±10	354± 6
	345	324	348		330	348		330				
NGC 2535	4100± 2	154± 5	120± 4	4100± 2	154± 5	120± 4	4100± 2	154± 5	120± 4	4102± 4	159± 7	140± 8
	144	118	144		118	144		144				
NGC 2770	1948± 2	373± 6	340± 3	1948± 2	373± 6	340± 3	1948± 2	373± 6	340± 3	1950± 3	385± 7	356± 5
	354	335	355		336	355		336				
IC 529	2262± 5	345±14	306± 7	2260± 5	348±15	310± 7	2262± 5	348±15	309± 7	2264± 7	370±17	333±12
	327	302	329		305	329		330				
NGC 3041	1408± 2	306± 7	278± 4	1408± 2	306± 7	279± 4	1408± 2	306± 7	279± 4	1406± 3	320±11	298± 5
	288	274	288		274	288		288				
UGC 5459	1112± 2	295± 4	266± 3	1109± 2	298± 4	273± 3	1112± 2	298± 4	272± 3	1111± 2	308± 5	288± 4
	277	262	279		269	280		280				
NGC 3254	1355± 1	442± 2	408± 1	1355± 1	443± 2	409± 1	1355± 1	444± 2	409± 1	1352± 1	458± 2	432± 2
	424	403	425		405	425		425				
NGC 3264	941± 1	160± 3	132± 2	940± 1	161± 2	134± 3	941± 1	161± 3	133± 3	939± 1	166± 3	147± 2
	151	129	152		132	152		152				
NGC 3338	1302± 1	360± 2	333± 2	1300± 1	363± 2	340± 2	1302± 1	363± 2	339± 2	1301± 1	370± 4	352± 2
	342	329	345		335	344		334				
NGC 3432	617± 4	267± 7		621± 4	275±11	259± 7	616± 6	272±12	254±12	617± 4	280±12	267± 7
	258				266	257		263				
NGC 3666	1063± 2	291± 6	263± 3	1063± 2	291± 6	264± 3	1063± 2	291± 6	264± 3	1063± 3	305±10	281± 4
	273	259	273		260	273		260				
NGC 3769	732± 4	249± 8		727± 4	255± 8	236± 8	732± 4	255± 7	236± 7	732± 4	259± 8	244± 7
	240				246	234		246				
NGC 3949	807± 4	295±11	255± 7	802± 4	301±12	265± 7	806± 4	300±13	264± 7	805± 6	320±23	287± 8
	277	251	283		261	282		282				
NGC 4100	1076± 6	419±15	382±11	1076± 7	419±15	382±11	1076± 6	419±15	382±11	1074±10	438±21	407±21
	401	377	401		378	401		378				
NGC 4144	265± 1	176± 3	157± 2	264± 1	177± 4	160± 2	265± 1	177± 3	159± 2	264± 2	183± 5	168± 3
	167	155	168		158	168		168				
NGC 4157	770± 2	429± 4	396± 3	774± 2	435± 4	406± 2	772± 2	433± 4	404± 3	774± 2	444± 7	421± 2
	411	392	417		402	415		415				
NGC 4183	930± 1	251± 3	235± 2	930± 1	251± 3	235± 2	930± 1	251± 3	235± 2	930± 2	258± 8	246± 3
	242	233	242		233	242		242				
NGC 4217	1028± 5	424±18	391± 7	1031± 5	426±20	397± 7	1028± 5	428±21	396± 7	1025± 7	446±16	414±11
	406	387	408		393	410		410				
NGC 4414	716± 6	422±13	383±11	716± 6	422±13	384±11	716± 6	422±13	384±11	715± 5	438±12	408±10
	403	379	404		380	404		404				
NGC 4534	801± 1	135± 1	119± 1	801± 1	135± 1	119± 1	801± 1	135± 1	119± 1	801± 1	141± 2	129± 1
	126	117	126		117	126		126				
NGC 4545	2732± 8	274±16	242±17	2735± 8	277±16	249±18	2732± 8	277±16	250±16	2732± 8	284±15	268±16
	256	274	258		245	258		258				
NGC 4814	2517± 3	382± 7	336± 5	2521± 3	387± 7	345± 6	2518± 3	385± 8	342± 5	2524± 4	402±11	374± 7
	363	332	368		341	367		367				
UGC 8146	670± 1	177± 2	156± 1	671± 1	178± 2	158± 1	670± 1	178± 2	157± 1	671± 1	190± 7	173± 2
	168	154	169		155	169		169				

Table 5. continued

Name (1)	V_{sys}^1 (2)	W_{20}^1 (3)	W_{50}^1 (4)	V_{sys}^2 (5)	W_{20}^2 (6)	W_{50}^2 (7)	V_{sys}^3 (8)	W_{20}^3 (9)	W_{50}^3 (10)	V_{sys}^4 (11)	W_{20}^4 (12)	W_{50}^4 (13)
		$W_{20}^{1,c}$ (14)	$W_{50}^{1,c}$ (15)		$W_{20}^{2,c}$ (16)	$W_{50}^{2,c}$ (17)		$W_{20}^{3,c}$ (18)	$W_{50}^{3,c}$ (19)			
NGC 5023	407± 1	195± 2	179± 2	406± 1	196± 3	180± 2	407± 1	196± 3	180± 2	407± 1	201± 4	189± 2
	186	176	176		187	178		187	178			
NGC 5205	1766± 2	260± 4	243± 3	1767± 2	261± 4	246± 3	1766± 2	261± 5	247± 3	1764± 2	269± 5	259± 4
	251	241	241		251	244		252	244		7	
NGC 5350	2321± 2	332± 4	295± 3	2324± 2	336± 4	304± 3	2321± 2	336± 4	302± 3	2322± 3	346± 6	322± 4
	313	290	290		318	300		318	298		7	
NGC 5351	3610± 1	443± 3	407± 2	3615± 1	449± 3	420± 2	3611± 1	449± 3	417± 2	3611± 2	456± 5	435± 3
	425	402	402		431	415		430	413			
NGC 5529	2895± 2	600± 3	557± 3	2886± 1	617± 3	575± 1	2892± 1	614± 3	573± 1	2892± 2	637± 3	600± 3
	582	552	552		599	571		595	569			
NGC 5678	1917± 7	428±15	390±14	1921± 8	435±17	399±15	1917± 8	433±16	398±14	1918±10	447±19	419±21
	410	385	385		417	395		415	394			
NGC 5783	2337± 3	279±13	255± 3	2335± 3	290±11	257± 4	2337± 3	281±13	257± 4	2335± 4	305±14	270± 5
	270	253	253		281	255		272	255			
NGC 5894	2466± 4	446± 9	414± 8	2468± 4	448± 9	417± 6	2467± 4	448± 9	417± 7	2468± 4	460±10	434± 8
	427	410	410		429	413		429	412			
NGC 5899	2599± 8	503±17	464±14	2596± 8	506±17	472±15	2600±12	506±17	473±17	2601± 8	518±16	500±16
	483	460	460		486	467		487	468			
NGC 5951	1779± 3	282± 6	265± 6	1778± 3	283± 7	267± 4	1779± 3	283± 6	267± 5	1779± 3	287± 5	276± 5
	273	262	262		274	265		274	265			
NGC 6207	852± 3	246± 8	227± 4	852± 3	246± 8	228± 4	852± 3	246± 8	228± 4	851± 2	252± 5	237± 4
	237	225	225		237	226		237	226			
NGC 6236	1280± 7	192±13	167±17	1279± 7	193±14	171±15	1280± 7	193±14	170±16	1278± 7	201±15	183± 13
	183	165	165		184	169		184	168			
NGC 6255	919± 2	204± 4	174± 3	918± 2	206± 5	177± 3	919± 2	205± 5	177± 3	918± 2	220± 6	194± 3
	195	171	171		197	175		196	175			
NGC 6339	2108± 4	234± 9	214± 8	2108± 4	235± 9	215± 8	2108± 4	234± 9	215± 8	2110± 7	247±14	225±12
	224	212	212		226	213		225	213			
NGC 6643	1489±18	396±33	348±38	1492±18	399±34	354±40	1490±19	399±33	352±42	1491±15	408±35	371±25
	378	344	344		381	350		380	348			
NGC 6689	490± 1	227± 4	207± 2	490± 1	227± 4	207± 2	490± 1	227± 4	207± 2	490± 2	235± 5	219± 3
	218	205	205		218	205		218	205			
UGC 11635	4804± 3	564± 9	486± 5	4801± 3	568±10	493± 5	4804± 3	569± 9	493± 5	4819± 7	585± 9	559± 9
	545	481	481		549	489		550	488			
UGC 11651	1523± 7	287±23	259± 9	1524± 6	289±20	263± 9	1523± 5	289±10	263± 9	1523± 6	300±12	281±12
	269	255	255		271	259		271	259			
UGC 11707	905± 1	205± 3	185± 2	907± 1	208± 3	189± 2	906± 1	207± 3	189± 2	906± 2	213± 5	200± 2
	196	183	183		199	187		198	187			
NGC 7177	1150± 5	319±10	294± 9	1150± 5	319±10	295± 9	1150± 5	319±10	295± 9	1151± 5	326±11	309±11
	300	290	290		300	290		301	290			
NGC 7497	1700± 3	304± 5	259± 6	1706± 2	312± 6	279± 4	1701± 2	311± 6	276± 4	1702± 3	325± 8	297± 4
	285	255	255		293	274		293	271			
NGC 7664	3477± 3	357± 8	324± 4	3476± 3	359± 8	326± 5	3477± 3	359± 8	327± 5	3477± 5	373±18	346± 7
	339	319	319		340	322		341	322			
NGC 7741	751± 2	212± 4	189± 3	750± 2	212± 4	191± 3	751± 2	213± 4	191± 3	752± 2	220± 8	203± 3
	203	187	187		203	189		204	189			
NGC 7753	5168± 6	380±10	324±16	5162± 6	385±10	348±13	5166± 6	385±10	341±14	5164± 5	398±11	372±10
	361	320	320		366	344		366	337			

Notes to Table 5

Column 1: Galaxy name

Columns 2–19: All values are expressed in units of km/s.

Columns 2,5,8,11: Systemic velocities determined from global profiles. Numbers indicate the method used (see text)

Columns 3 and 4: HI linewidths determined from method 1 (see text)

Columns 6 and 7: HI linewidths determined from method 2 (see text)

Columns 9 and 10: HI linewidths determined from method 3 (see text)

Columns 12 and 13: HI linewidths determined from method 4 (see text)

Columns 14–19: Same as Columns 3,4,6,7,9 and 10, respectively, but corrected for instrumental broadening (see text)

$$W_l = W_{l,\text{obs}} - F_l(r) = W_{l,\text{obs}} + (a \cdot l + b) \cdot r, \quad (11)$$

where W represents a linewidth in km/s and l is the level in percentages ($l = 20$ or 50), r the velocity resolution in km/s and $a (= 0.014)$ and $b (= -0.83)$ are coefficients. The linewidths corrected in this way are listed in Cols. 14–19 of Table 5. The linewidths of Cols. 14 and 15 of Table 5 are

instrumental broadening was applied to the raw data, the systematic difference disappeared.

We have compared our measurements with those listed in the LEDA. To make a fair comparison, we have used only parameters measured with the first method, which was adopted in the LEDA and by Bottinelli et al. (1990). We have corrected the observed linewidths for instrumental broadening following Bottinelli et al. (1990), according

Table 6. Maximum rotation velocities

Name (1)	$V_{\max} \sin i$ km/s (2)	V_{\max} km/s (3)	Name (1)	$V_{\max} \sin i$ km/s (2)	V_{\max} km/s (3)	Name (1)	$V_{\max} \sin i$ km/s (2)	V_{\max} km/s (3)
NGC 7817	165± 9	167	NGC 3264	53± 5	58	NGC 5529	256± 8	256
NGC 100	98± 3	98	NGC 3338	143± 5	174	NGC 5678	171± 9	185
NGC 514	113± 4	197	NGC 3432	120± 3	122	NGC 5783	116± 4	145
NGC 691	165± 9	234	NGC 3666	127± 9	130	NGC 5894	187±13	187
IC 167	62± 7	82	NGC 3769	114± 7	117	NGC 5899	178±12	192
NGC 697	199± 6	206	NGC 3949	108± 8	131	NGC 5951	120± 4	120
NGC 772	221±11	260	NGC 4100	165± 8	170	NGC 6207	105± 6	113
NGC 803	114± 5	124	NGC 4144	78± 5	79	NGC 6236	73± 6	87
NGC 918	116± 4	140	NGC 4157	184± 9	184	NGC 6255	94± 4	102
NGC 949	85± 4	106	NGC 4183	105± 3	105	NGC 6339	90± 7	108
NGC 1171	116± 5	126	NGC 4217	186± 6	187	NGC 6643	141±14	158
IC 381	127±18	151	NGC 4414	179± 6	216	NGC 6689	88± 7	90
UGC 3137	90± 6	90	NGC 4534	53± 3	87	UGC 11635	208±10	223
NGC 2357	148± 7	148	NGC 4545	106±10	126	UGC 11651	114± 8	117
NGC 2535	36± 4	41	NGC 4814	143± 8	196	UGC 11707	88± 3	103
NGC 2770	148± 6	152	UGC 8146	79± 7	79	NGC 7177	125± 9	161
IC 529	137± 3	151	NGC 5023	82± 4	82	NGC 7497	122± 4	128
NGC 3041	119± 8	153	NGC 5205	112± 4	134	NGC 7664	157± 5	185
UGC 5459	132± 7	132	NGC 5350	135± 6	215	NGC 7741	73± 5	100
NGC 3254	191± 8	196	NGC 5351	151± 8	178	NGC 7753	152± 7	208

Notes to Table 6

Column 1: Galaxy name

Column 2: Maximum rotation velocity, uncorrected for inclination

Column 3: Maximum rotation velocity, corrected for inclination

plotted against those taken from the LEDA in Fig. 2; the agreement between two measurements is quite good. The mean differences are small: $\langle W_{20}(\text{WSRT}) - W_{20}(\text{LEDA}) \rangle = -5 \pm 15$ and $\langle W_{50}(\text{WSRT}) - W_{50}(\text{LEDA}) \rangle = -6 \pm 11$ km/s. The mean difference in the systemic velocities is also small: $\langle V_{\text{sys}}(\text{WSRT}) - V_{\text{sys}}(\text{LEDA}) \rangle = 1 \pm 7$ km/s. The least-squares fits to the data points in Figs. 2a and 2b give the standard deviations with respect to the fitted lines as 0.02 dex for both cases. The resulting fits are given below:

$$\begin{aligned} \log W_{20}^{\text{LEDA}} &= 0.98 (\pm 0.02) \log W_{20}^{\text{WSRT}} + 0.05 (\pm 0.05), \\ \log W_{50}^{\text{LEDA}} &= 0.98 (\pm 0.01) \log W_{50}^{\text{WSRT}} + 0.04 (\pm 0.04). \end{aligned} \quad (12)$$

In summary, we confirm that there is no major systematic difference between WSRT and single-dish measurements of linewidths and systemic velocities when homogeneous procedures are applied.

3.3. Maximum rotational velocities

First-order rotation curves have been derived from the position-velocity maps by taking the central velocity of the most extreme component from two-component gaussian

fits to the HI profile at each position along the resolution axis as the projected rotation velocity. For a discussion of this approach, see Begeman (1987). These rotation curves can be compared with those derived from long-slit spectroscopy using, for instance, H α emission lines. Both the short WSRT observations and long-slit spectroscopy give essentially one-dimensional information along one particular direction. The rotation curves derived in this way could be different from the true rotation curve if the inclination and/or position angle is a strong function of the radius (e.g. warp, etc.), especially in the outer parts.

Maximum rotation velocities have been determined from the rotation curves. The uncertainty in the maximum rotation velocity has been estimated from the root-mean-square of the mean gaussian-fits error in the central velocities of the extreme components and the velocity difference between the approaching and receding sides. Maximum rotation velocities, observed and corrected for inclination, are listed in Table 6.

3.4. HI diameters and surface density profiles

The HI surface density profiles, σ_{HI} , have been derived following the method described in Warmels (1986, 1988b).

As a first step, the position-velocity maps have been integrated over the radial velocity direction, resulting in HI strip integrals, Σ_{HI} (see top left-hand panel of Fig. 4). In order to get the HI surface density profiles, the iterative deconvolution method described in Lucy (1974) has been applied to the HI strip integrals, assuming an axisymmetric HI distribution, of which the equatorial plane coincides with that of the stellar disc of the galaxy. Optically determined position angles and inclinations have been used for the calculation. The HI surface density profiles for 60 galaxies are presented in Fig. 3.

The surface density profiles have been used to define the sizes and effective densities of the HI discs. The HI diameters, D_{HI} , have been defined with the ‘face-on’ isophotal surface densities of HI at the level of $1 M_{\odot}/\text{pc}^2$, as did Warmels (1986, 1988b), Broeils (1992) and Broeils & van Woerden (1994). The radii enclosing half of the total HI flux are taken as the effective HI radii, R_{eff} , and the local HI surface densities at R_{eff} as the effective HI surface densities. The resulting values are listed in Table 4.

3.5. Position-velocity maps

In Fig. 4 we present position-velocity maps, global HI profiles and strip integrals. We have adopted the format of the atlas of Broeils’ (1992, see Fig. A1 in Sect. 2) for the presentation of our results. The position-velocity maps are presented in the bottom left panel of each figure. Contours indicate lines of equal intensity; the levels are -4σ , -2σ (dotted lines), 2σ , 4σ , and continued in steps of 2σ (solid lines). The vertical dotted line represents the centre of each galaxy and the horizontal line the systemic velocity. The arrows indicate the positions of the maximum rotation velocities. The bottom right-hand panel of each figure presents the global HI profiles. The arrow indicates the systemic velocity and the error bar at the bottom right-hand corner shows the velocity resolution. The HI strip integrals are given in the top left-hand panel in units of $\text{mJy km s}^{-1} \text{arcsec}^{-1}$. The arrows represent the uncorrected optical radius ($D_{25}/2$) and the error bar indicates the HPBW of the integrated antenna pattern. The galaxy name and the direction of the position angle of the resolution axis (e.g. NE stands for northeast) are given at the top of this panel. The morphological type and the position angle of the resolution axis of each galaxy are given in the top right-hand corner. In some cases, the position angles of the optical major axis are considerably different from the position angle of the resolution axes: 137° vs. 8° for NGC 803, 28° vs. 5° for NGC 5951, 18° vs. 165° for UGC 11651, and 18° vs. 170° for NGC 7741.

Acknowledgements. We wish to thank Renzo Sancisi, Adrick Broeils and Marc Verheijen for useful comments on the original manuscript and for advice on the data reduction, and Renée

Kraan-Korteweg for providing her computer programme of the Virgocentric infall model which was used to determine distances to galaxies in this study. We also would like to thank Arthur Coolen for help with map making procedures (LINE-JOB), and Kor Begeman and Martin Vogelaar for making GIPSY tasks suitable for the data reduction of short WSRT observations. M.-H. Rhee is grateful to the Netherlands Foundation for Research in Astronomy (ASTRON) and the Netherlands Organization for Scientific Research (NWO) for their support.

References

- Aaronson M., Huchra J., Mould J.R., et al., 1982, ApJS 50, 241
- Allen R.J., Ekers R.D., Terlouw J.P., 1985, in: Di Gesù V., et al. (eds.) *Proceedings of the International Workshop on Data Analysis in Astronomy*. Plenum, London, p. 271
- Begeman, K.G., 1987, Ph.D. Thesis, University of Groningen
- Bicay M.D., Giovanelli R., 1986, AJ 91, 705
- Bothun G.D., Aaronson M., Schommer R., et al., 1985, ApJS 57, 423
- Bottinelli L., Gouguenheim L., Fouqué P., Paturel G., 1990, A&AS 82, 391
- Broeils A.H., 1992, Ph.D. Thesis, University of Groningen
- Broeils A.H., van Woerden H., 1994, A&AS 107, 129
- Davis L.E., Seaquist E.R., 1983, ApJS, 53, 269
- de Vaucouleurs G., de Vaucouleurs A., Corwin Jr. H.G., et al., 1991, *Third Reference Catalogue of Bright Galaxies*. Springer-Verlag, New York (RC3)
- Dickel J.R., Rood H.J., 1980, AJ, 85, 1003
- Fouqué P., Bottinelli L., Gouguenheim L., Paturel G., 1990, ApJ 349, 1
- Haynes M.P., Giovanelli R., 1984, AJ 89, 758
- Högberg J.A., 1974, A&AS 15, 417
- Högberg J.A., Brouw W.N., 1974, A&A 33, 298
- Huchtmeier W.K., Richter O.-G., 1989, *A General Catalog of HI Observations of Galaxies*. Springer-Verlag, New York
- Kent S.M., 1984, ApJS 56, 105
- Kent S.M., 1986, AJ 91, 1301
- Kraan-Korteweg R.C., 1986, A&AS 66, 255
- Lucy L.B., 1974, AJ 79, 745
- Oosterloo T.A., 1988, Ph.D. Thesis, University of Groningen
- Oosterloo T.A., Shostak S., 1993, A&AS 99, 379
- Pierce M.J., Tully R.B., 1988, ApJ 330, 579
- Richter O.-G., Sancisi R., 1994, A&A 290, L9
- Rubin V.C., Burstein D., Ford W.K.Jr., Thonnard N., 1985, ApJ 289, 81
- Sullivan W.T.III., Bothun G.D., Bates B., Schommer R., 1981, AJ 86, 919
- Tully R.B., 1988, *Nearby Galaxies Catalog*. Cambridge University Press, Cambridge
- Tully R.B., Fisher J.R., 1977, A&A 54, 661
- Tully R.B., Fouqué P., 1985, ApJS 58, 67
- van Someren Greve H.W., 1974 A&AS 15, 343
- Warmels R.H., 1986, Ph.D. Thesis, University of Groningen
- Warmels R.H., 1988a, A&AS 72, 57
- Warmels R.H., 1988b, A&AS 72, 427

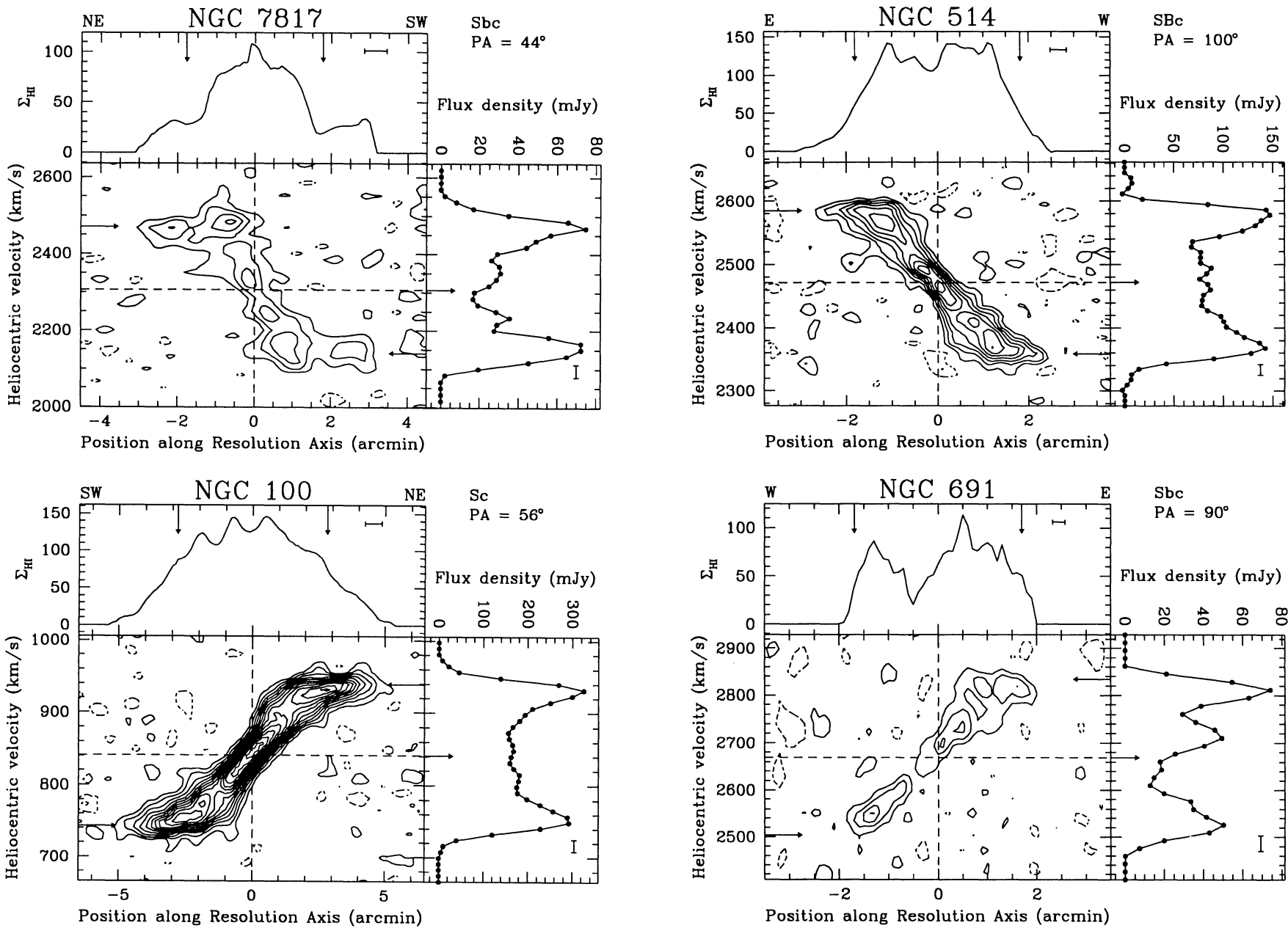


Fig. 4. Position-velocity maps (bottom left panel), global HI profile (bottom right panel), and strip integrals (top left panel). In the top right panel, Hubble type and the position angle of the resolution axis of each galaxy are shown

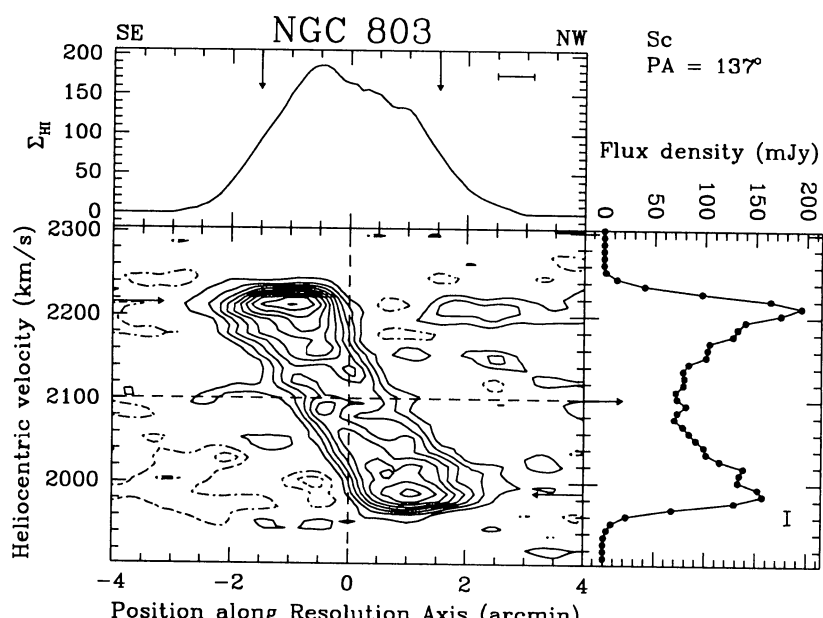
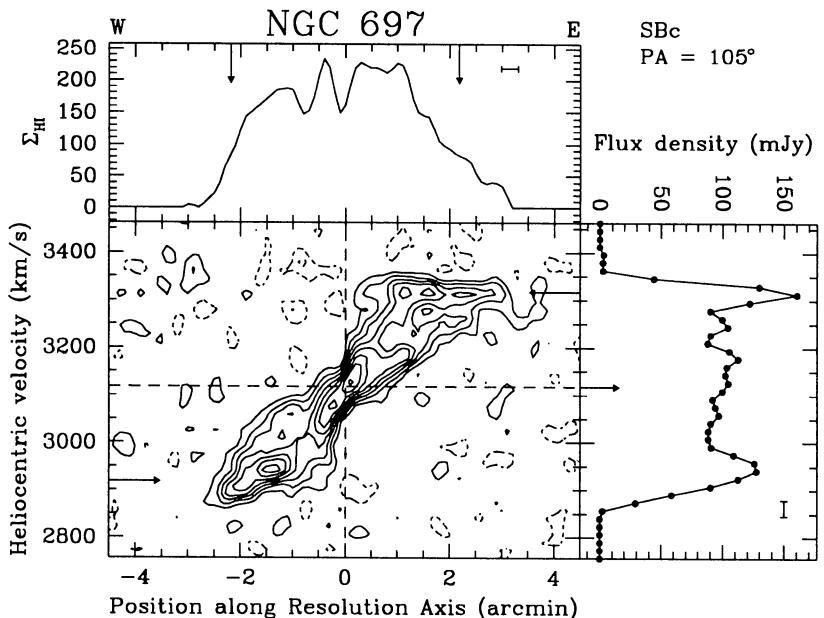
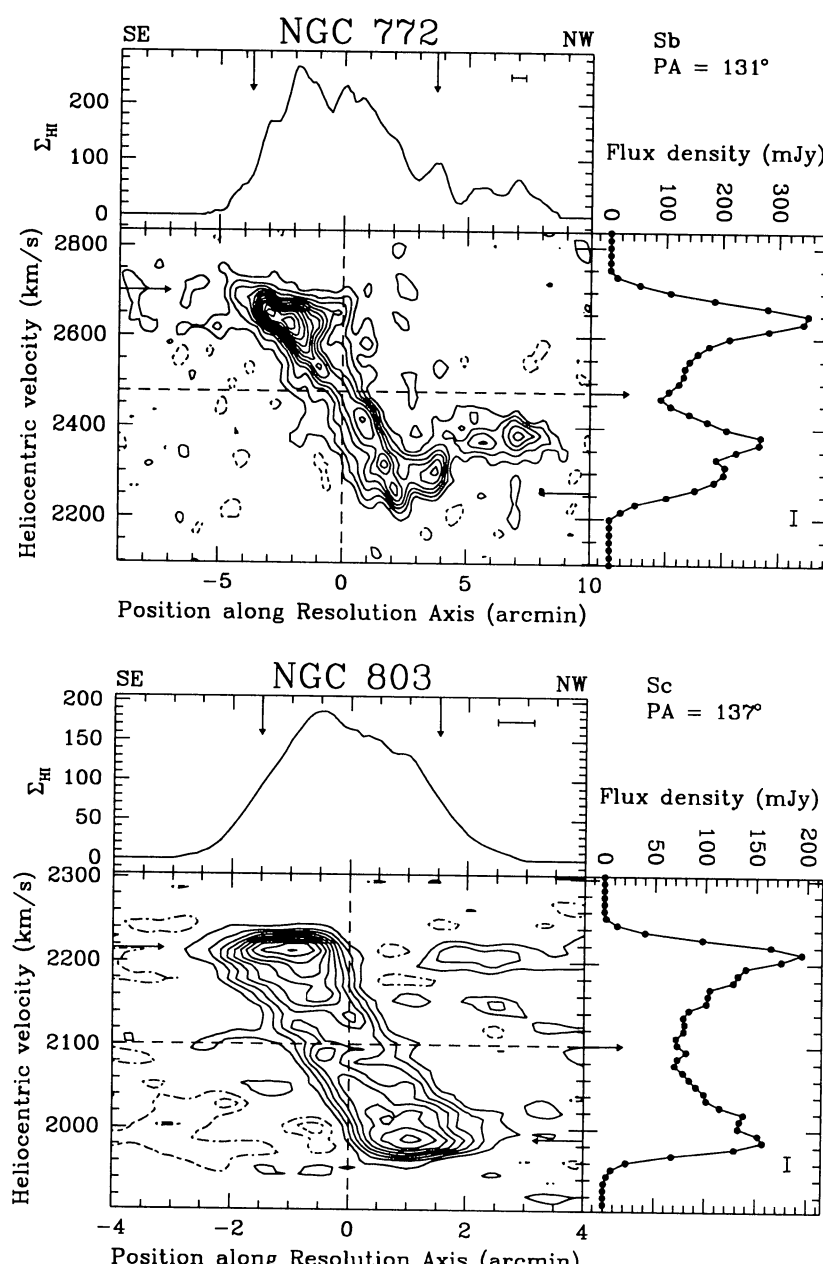
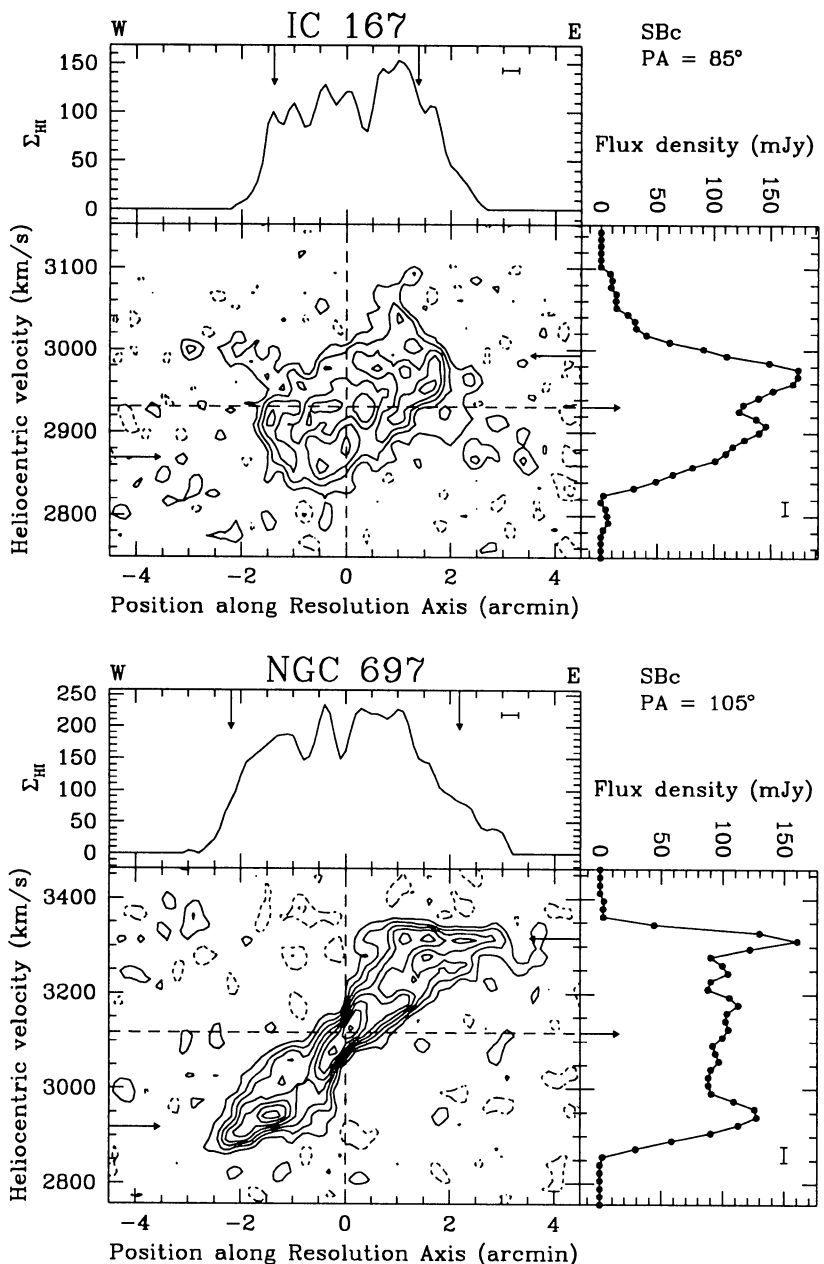


Fig. 4. continued

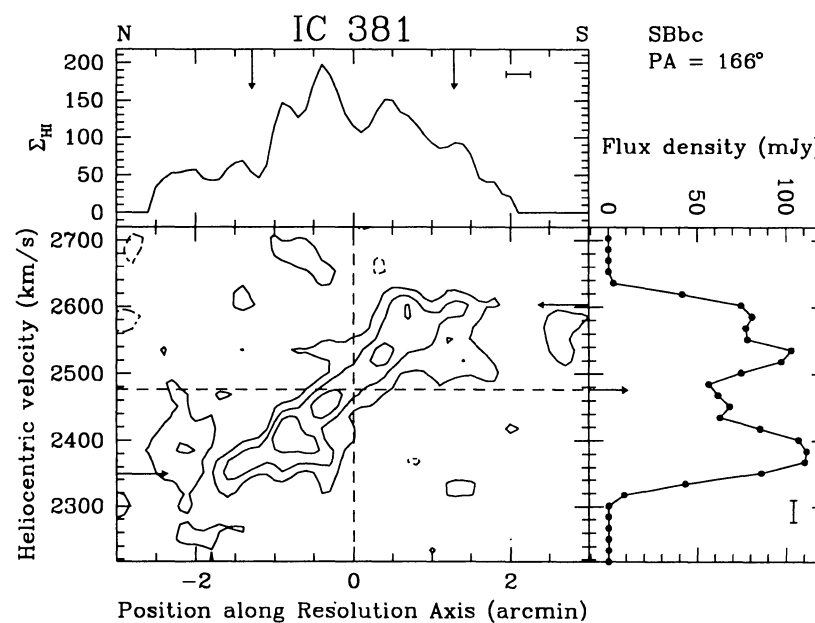
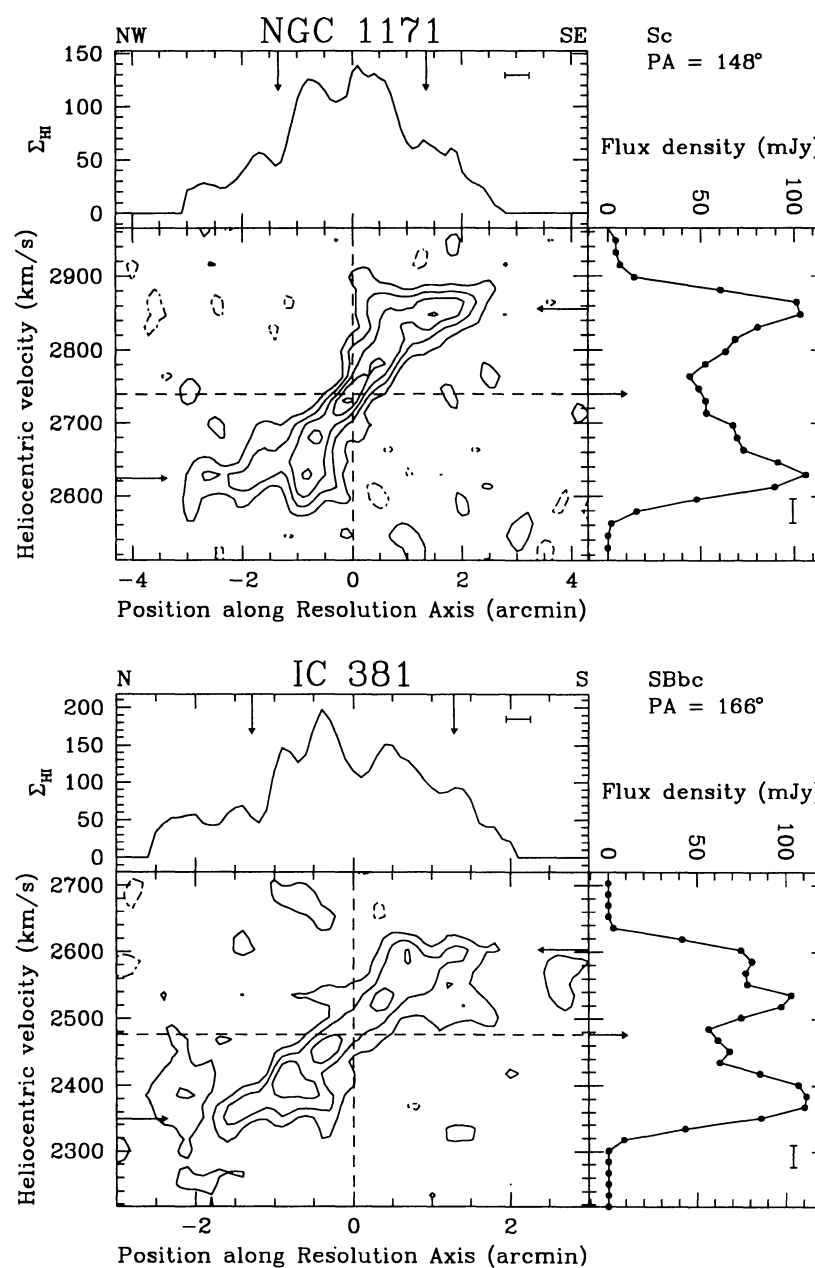
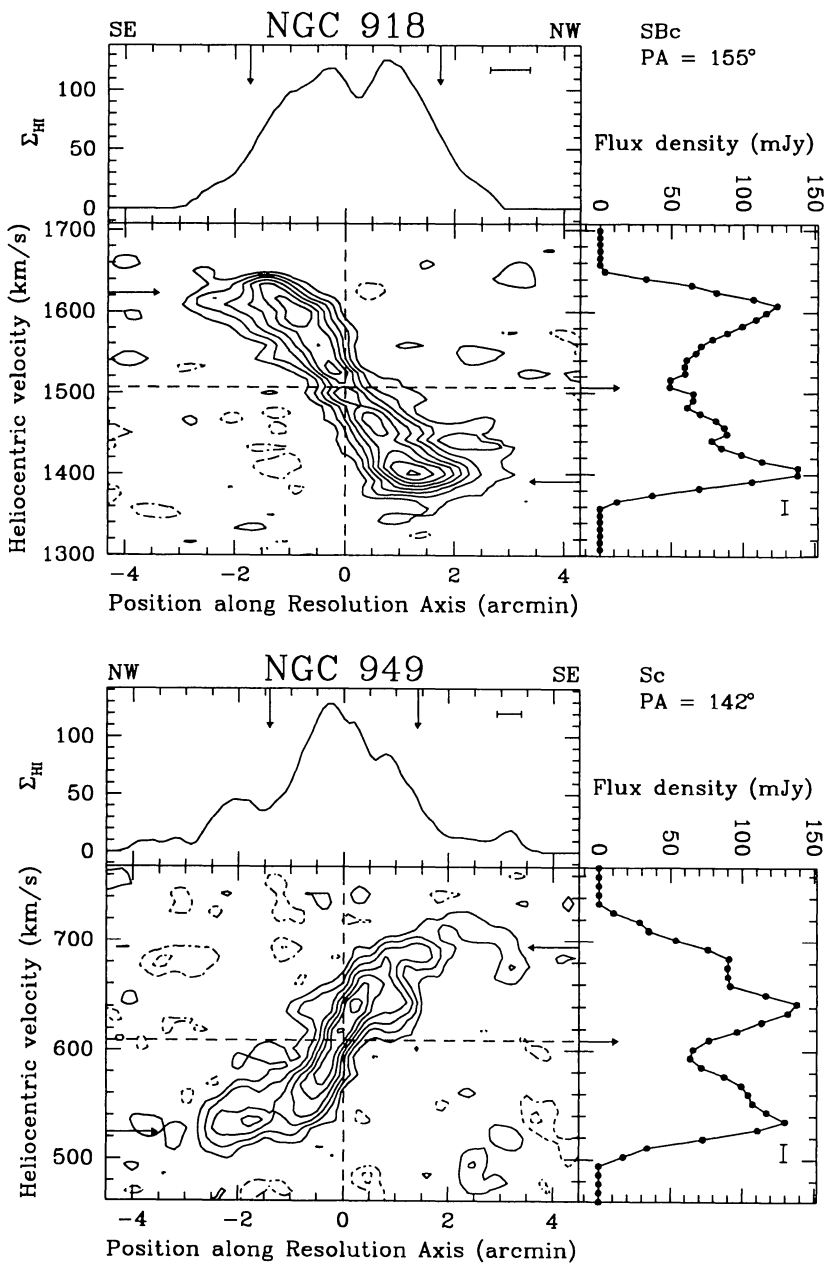


Fig. 4. continued

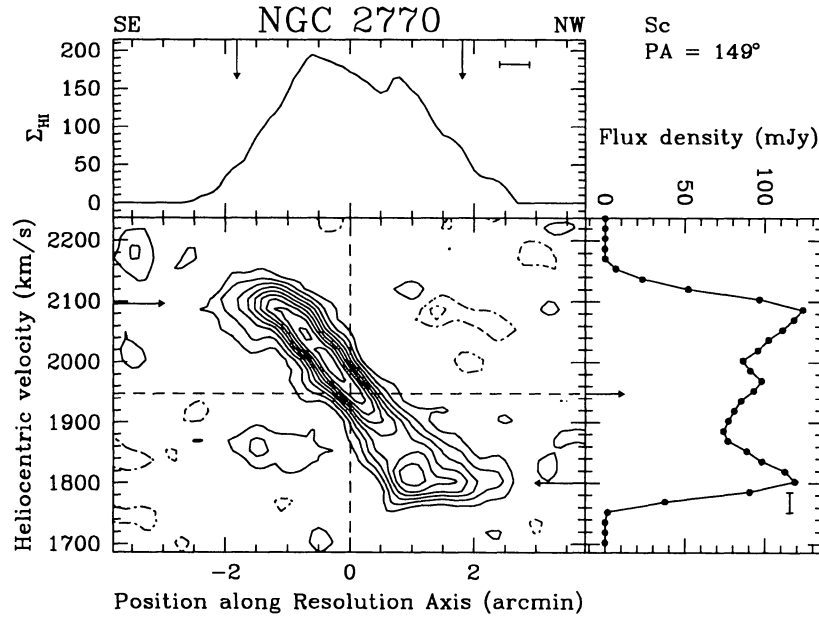
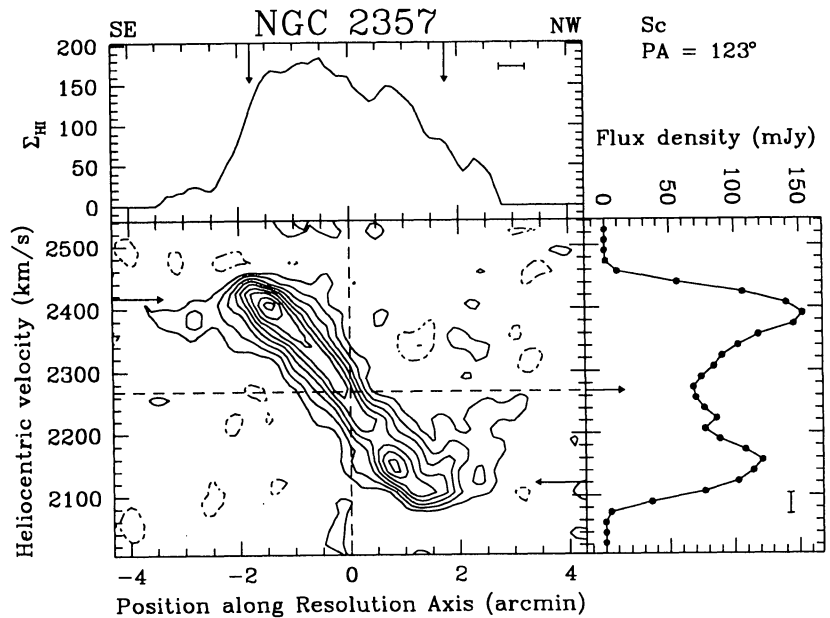
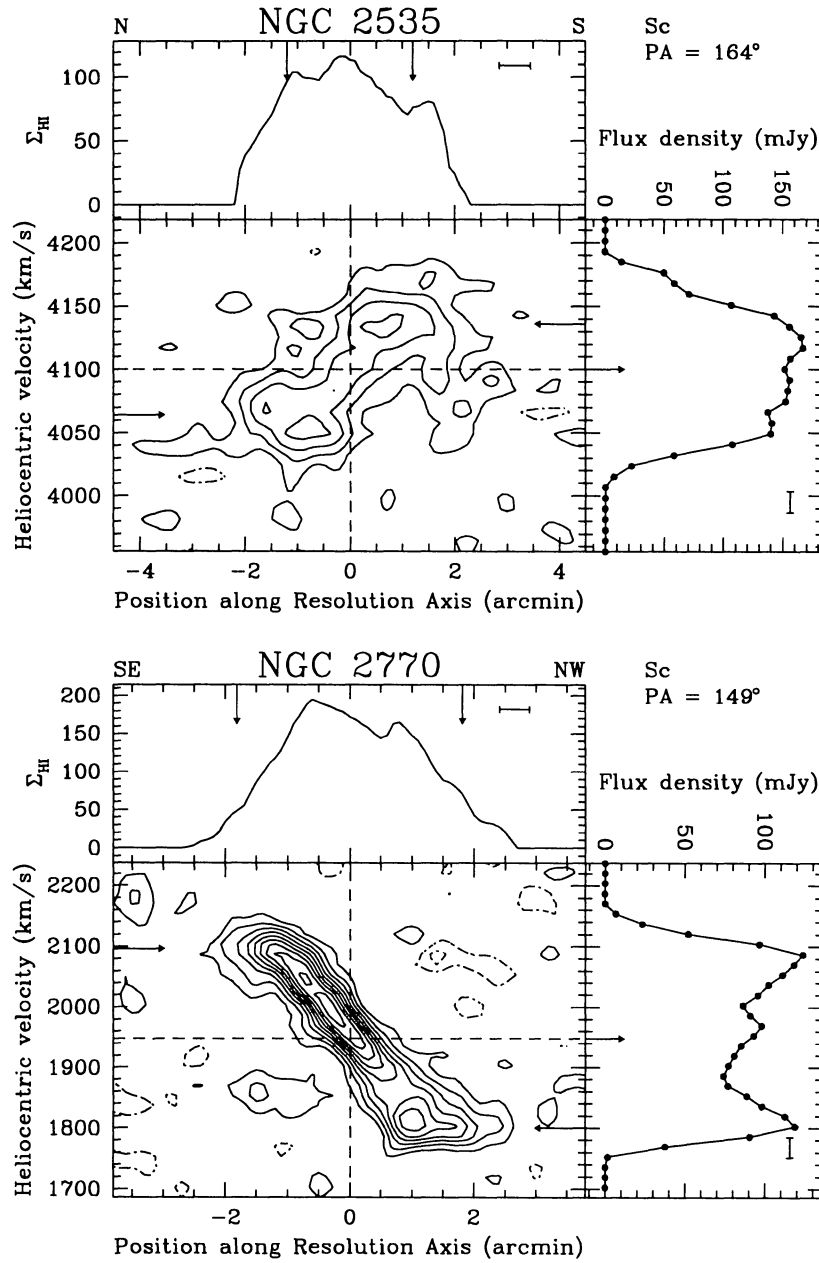
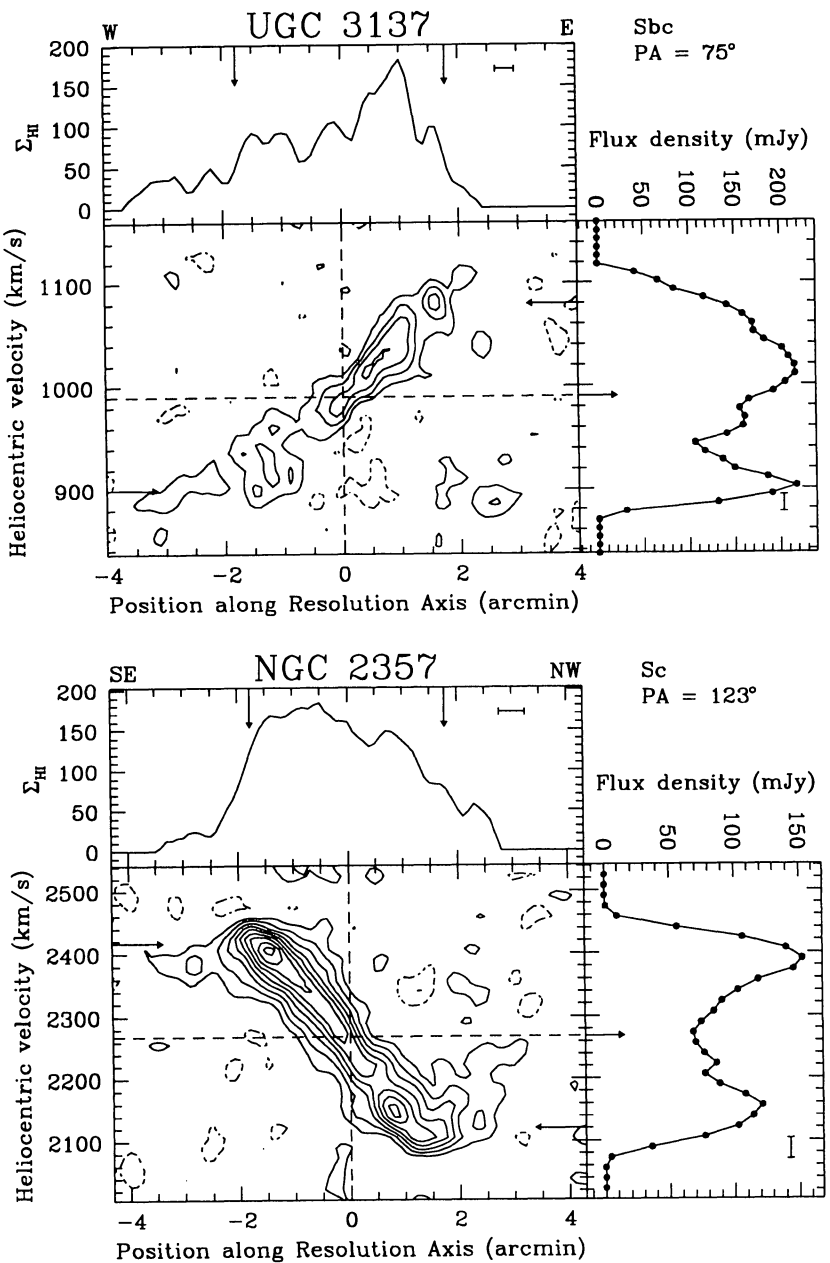


Fig. 4. continued

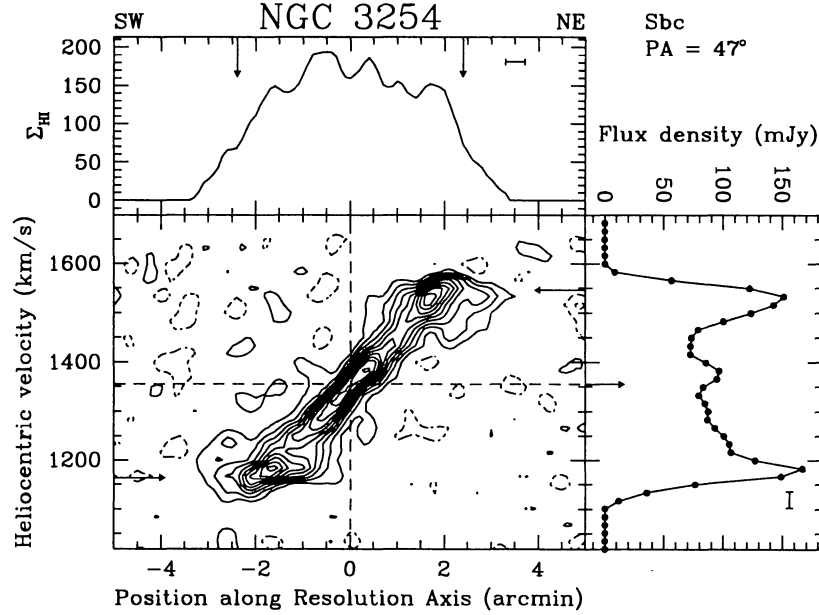
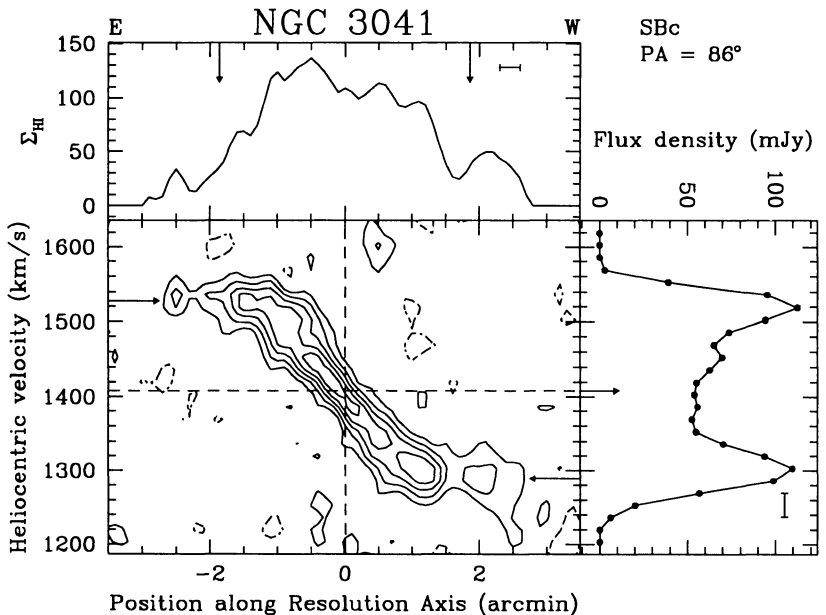
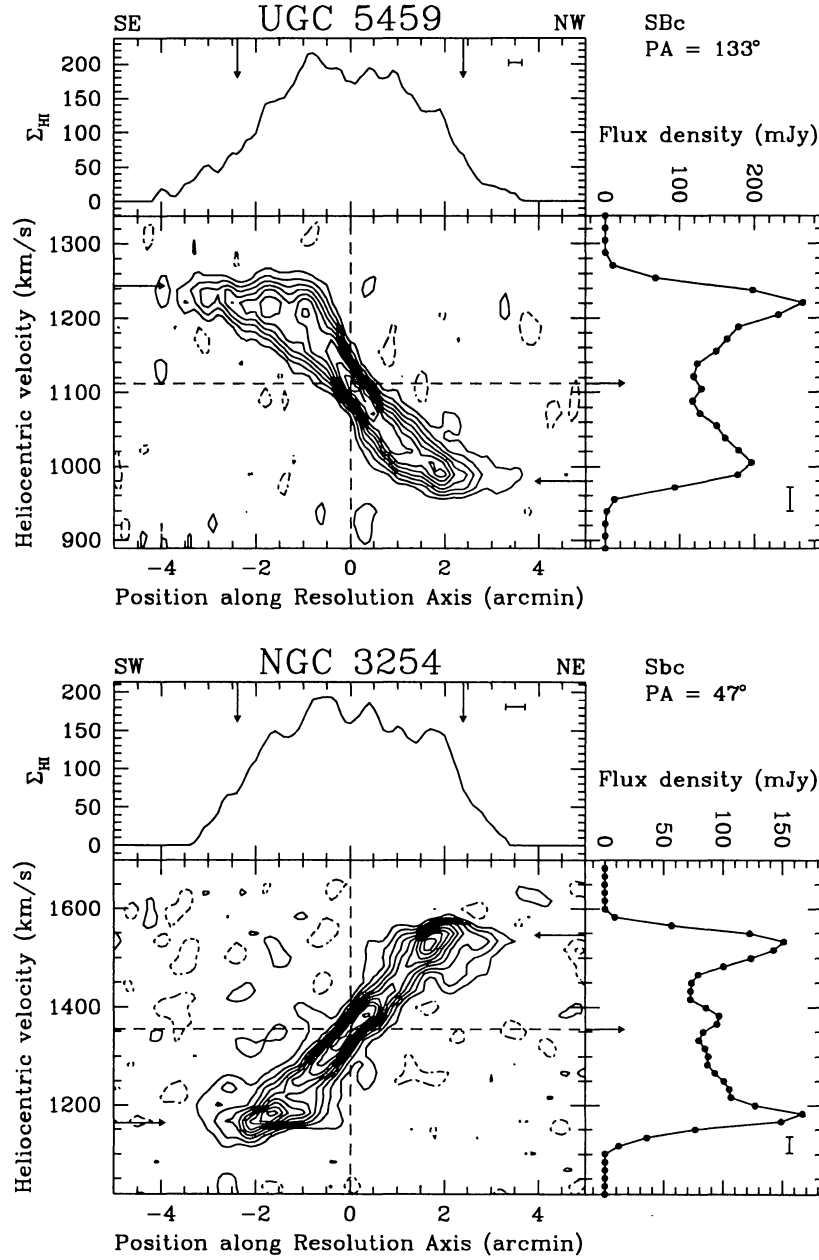
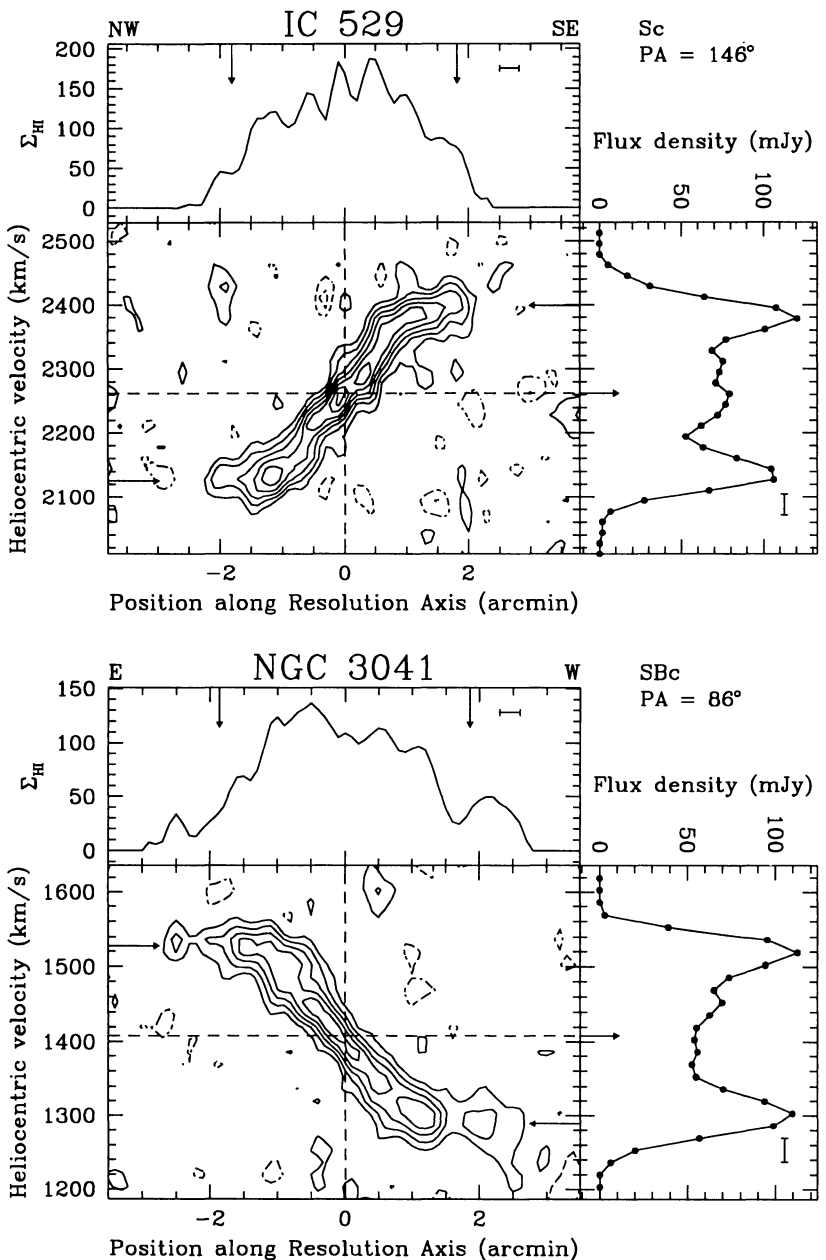


Fig. 4. continued

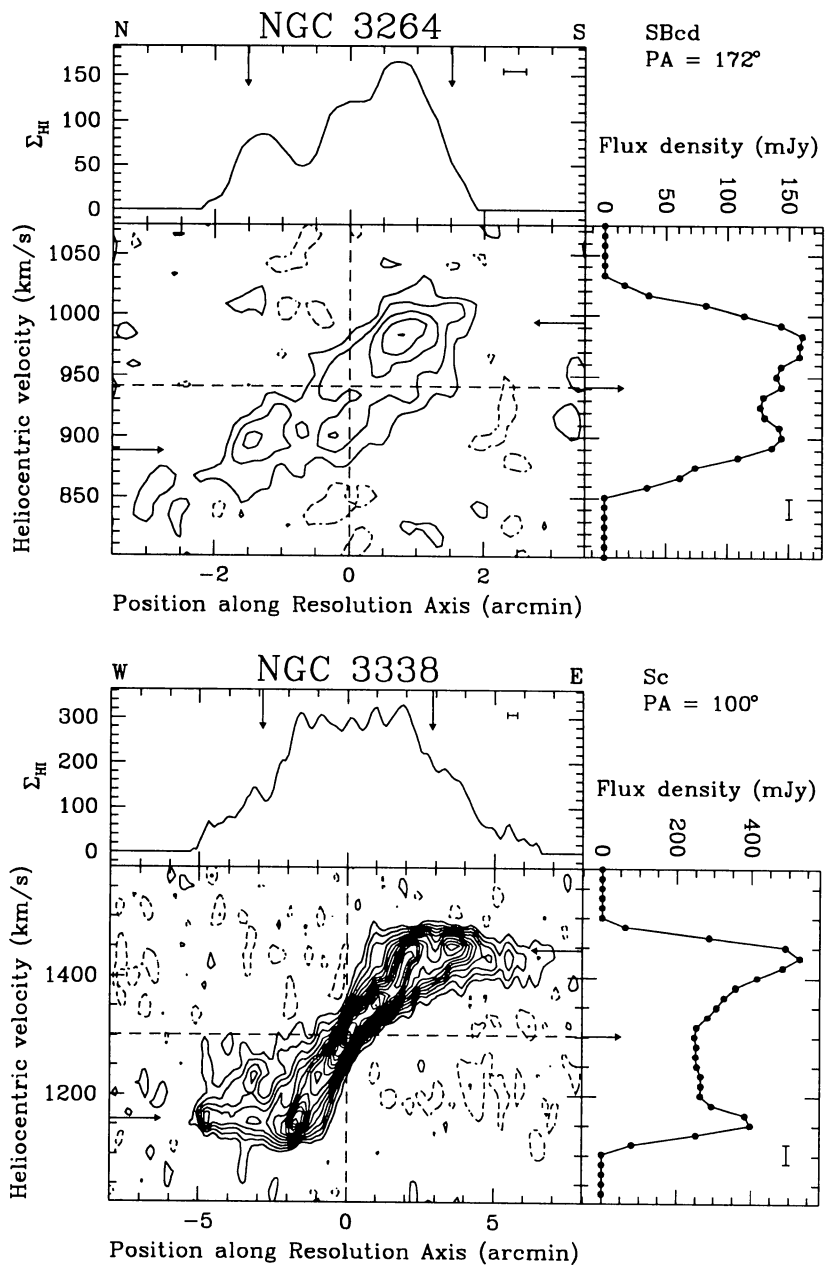


Fig. 4. continued

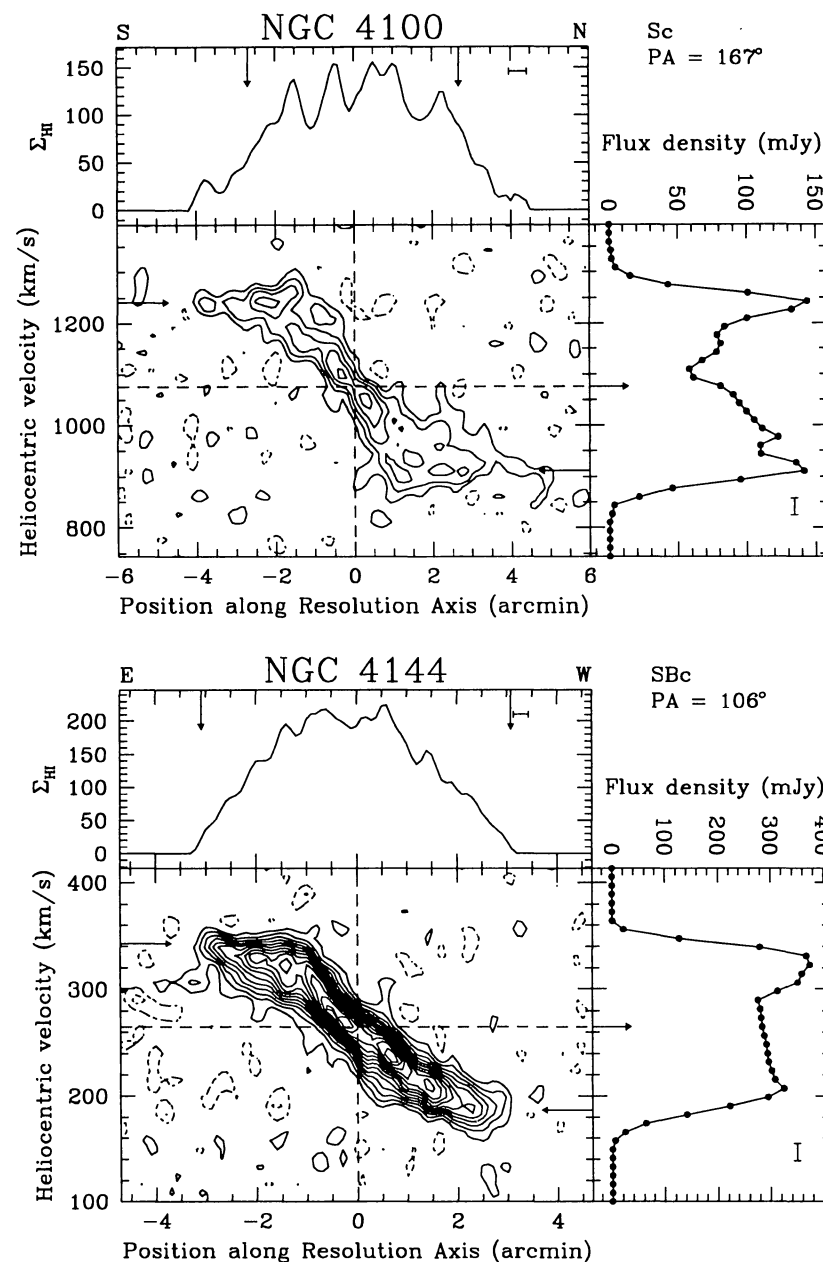
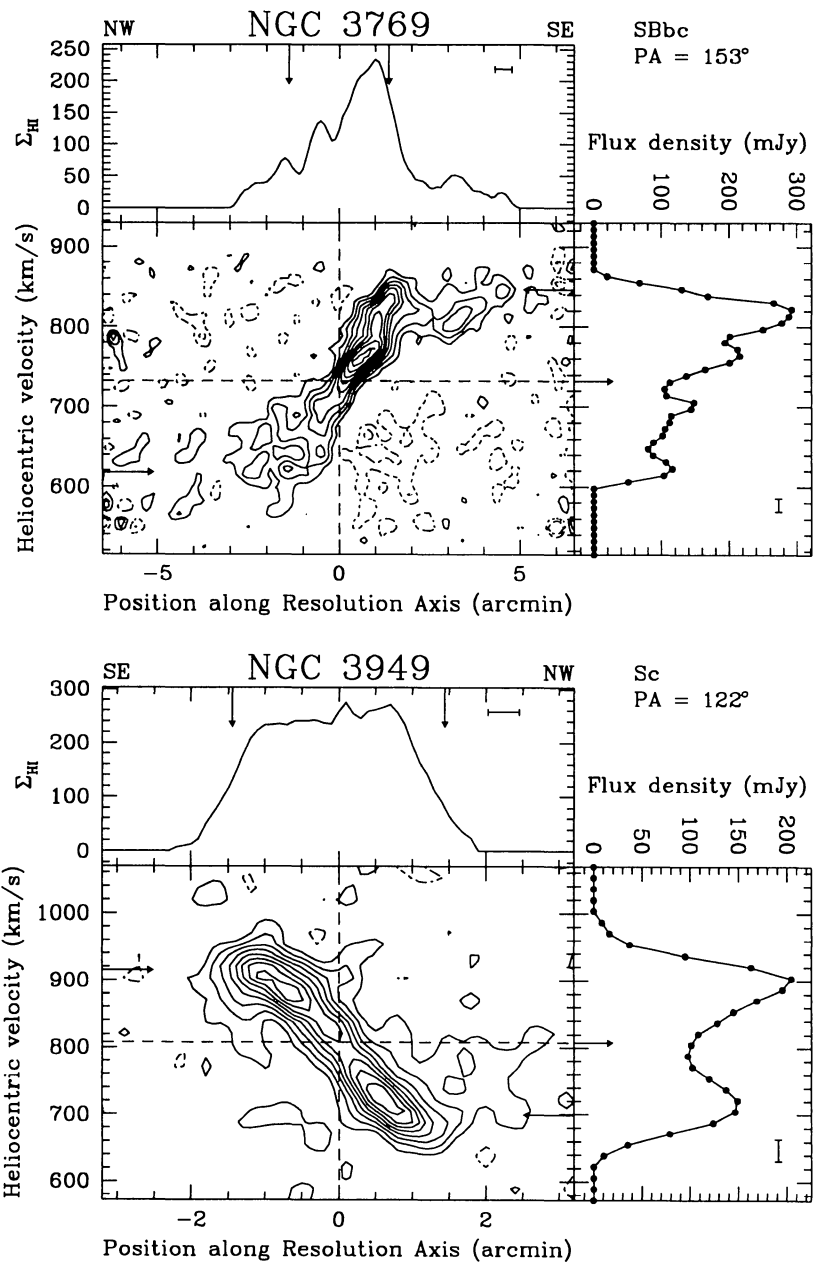


Fig. 4. continued

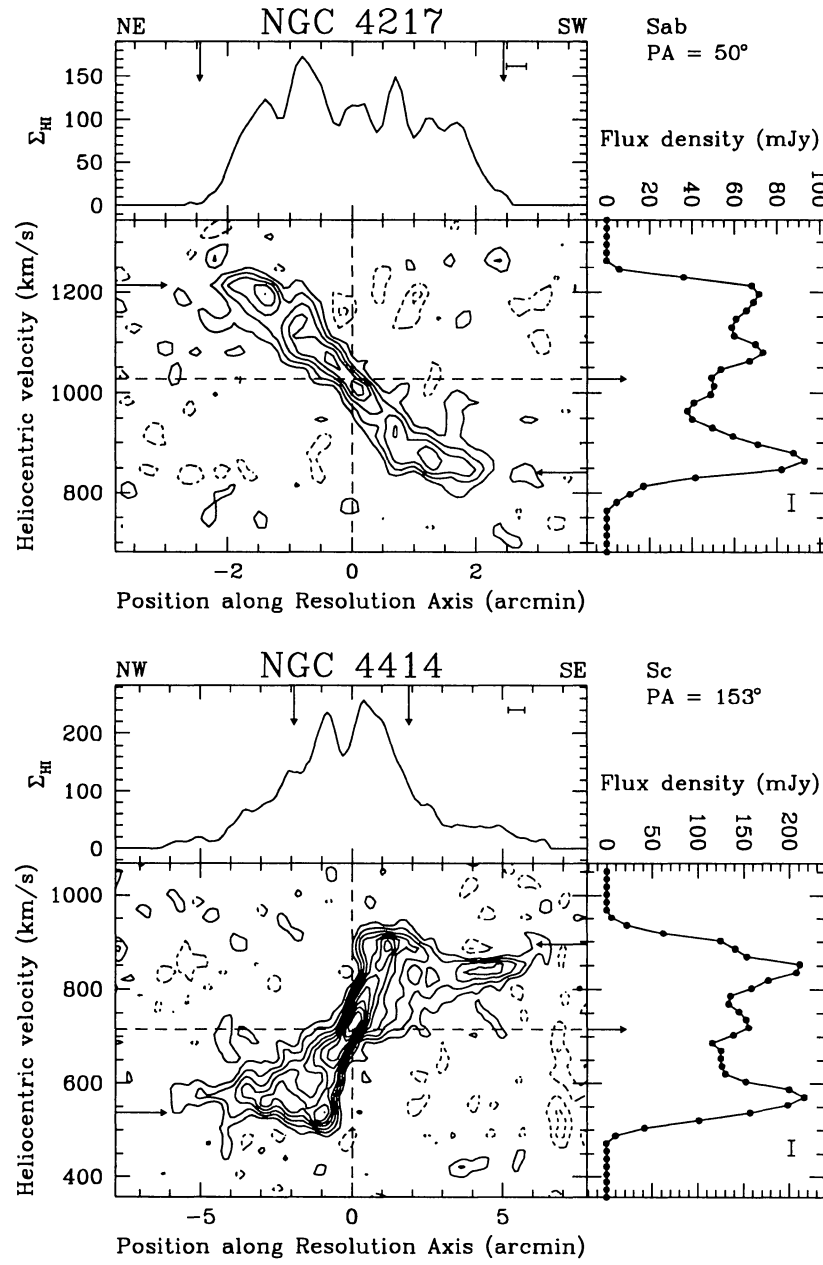
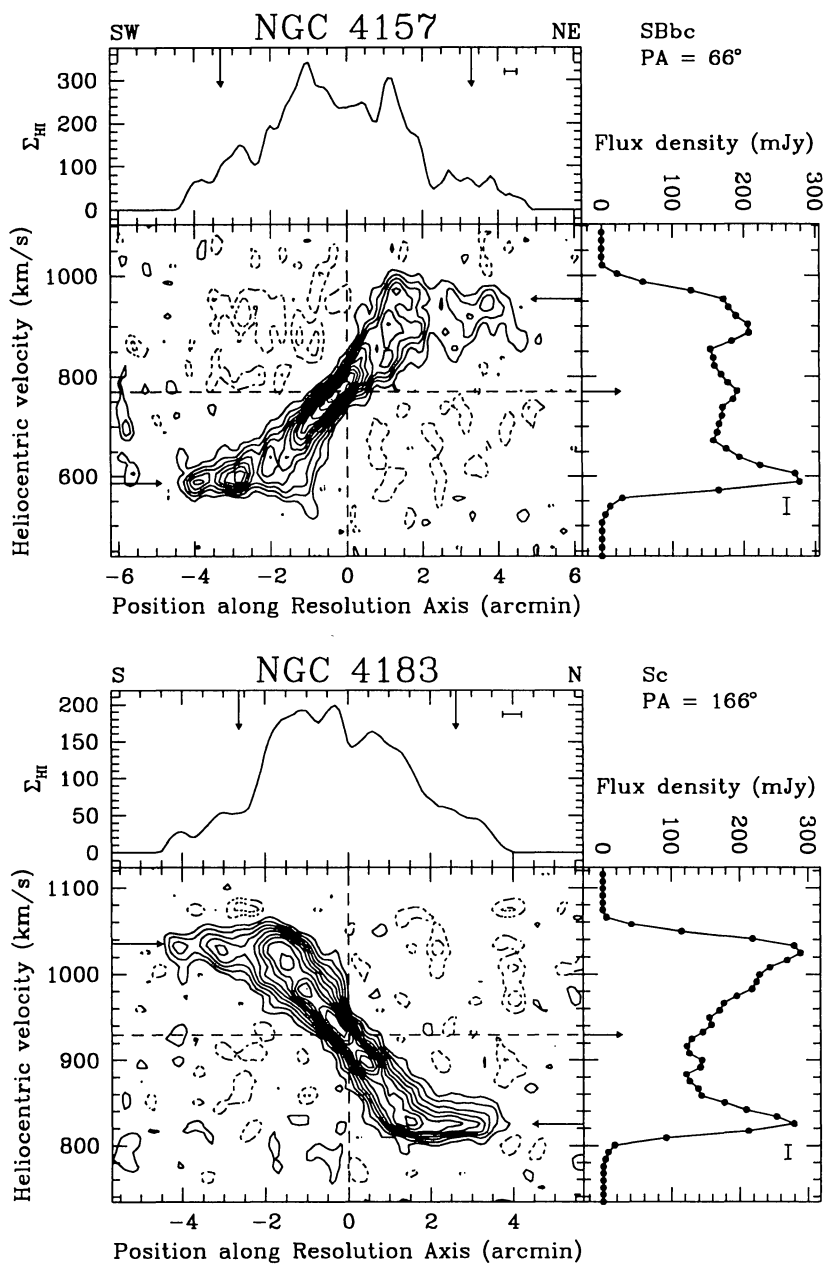


Fig. 4, continued

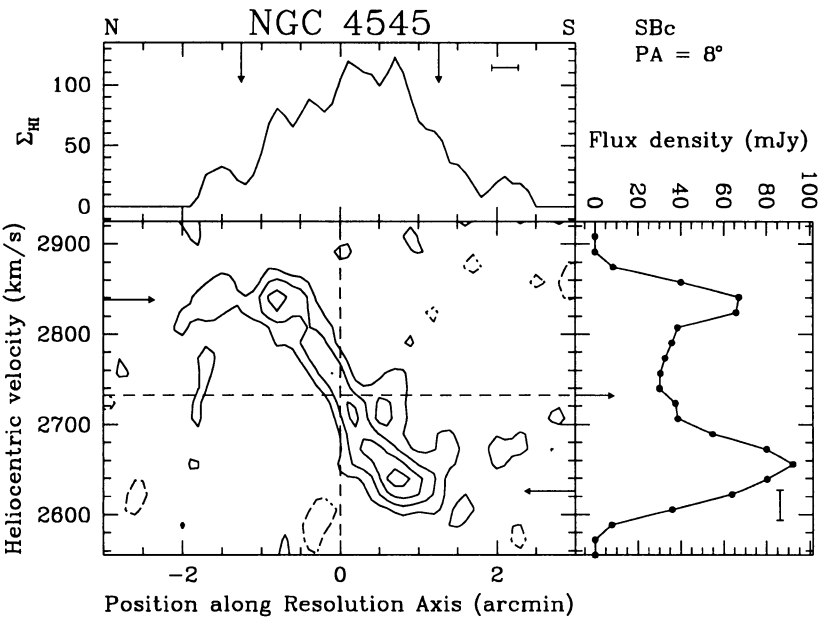
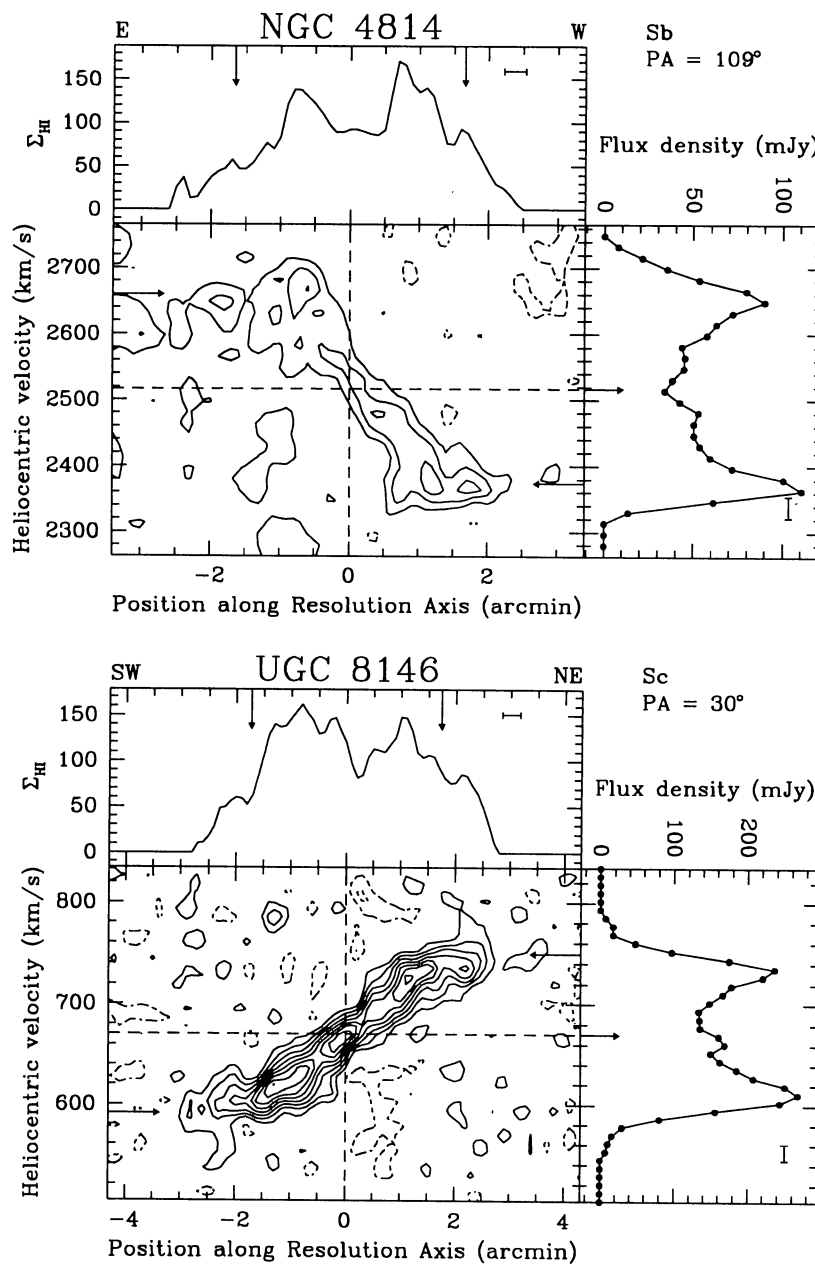
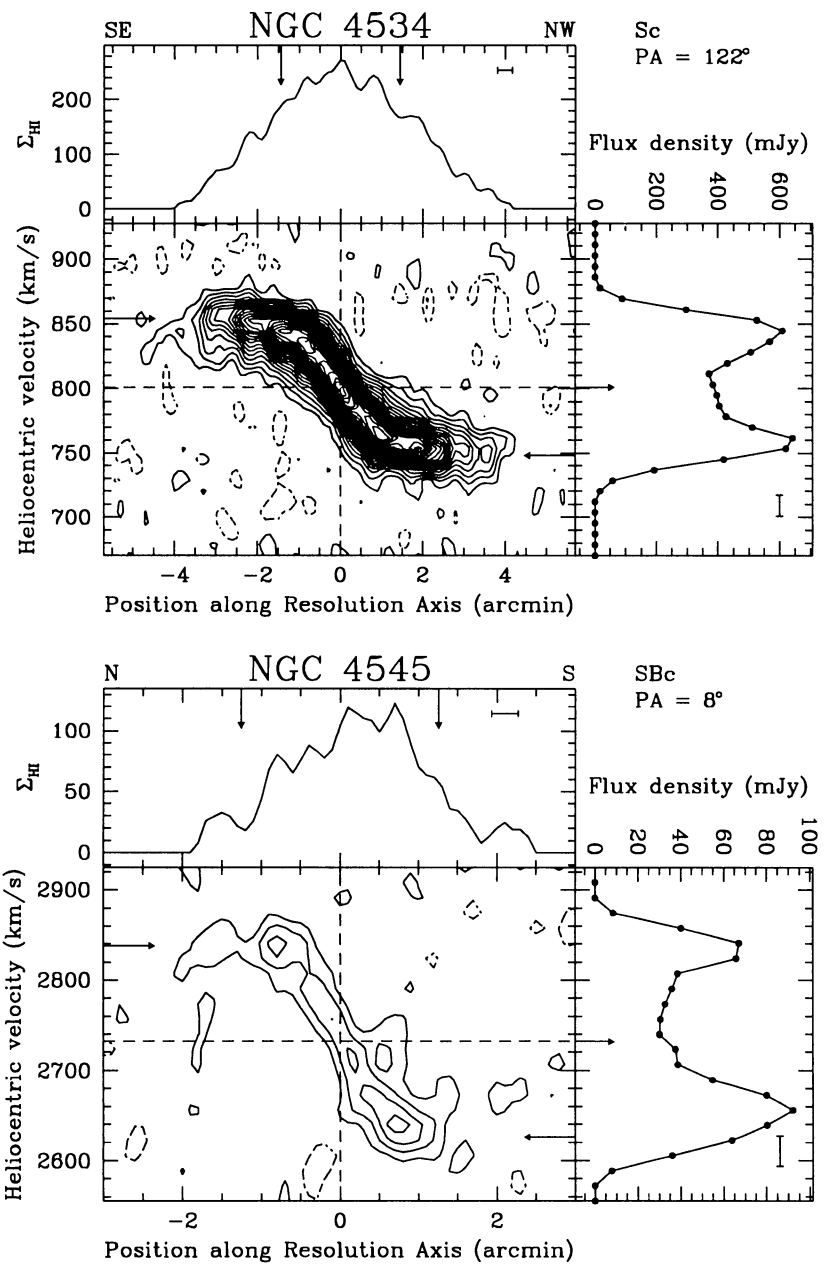


Fig. 4. continued

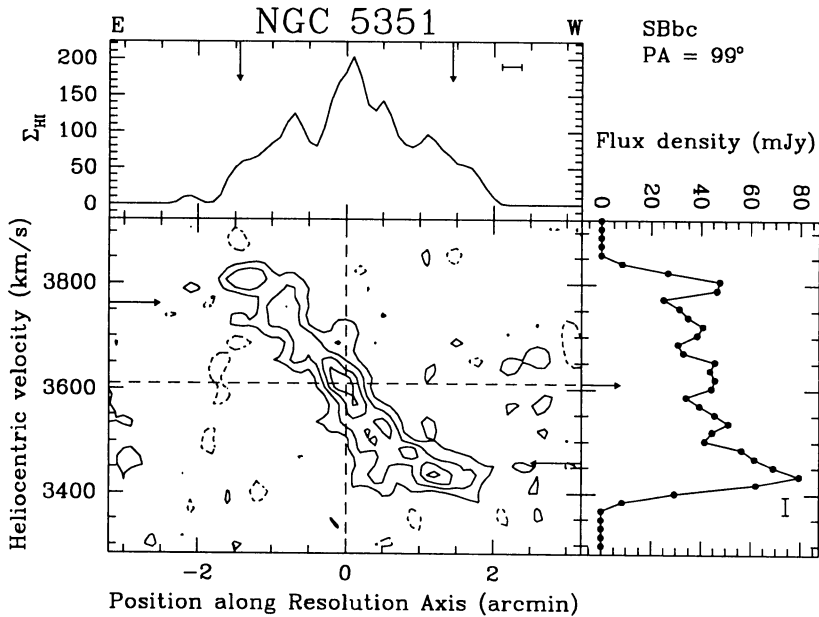
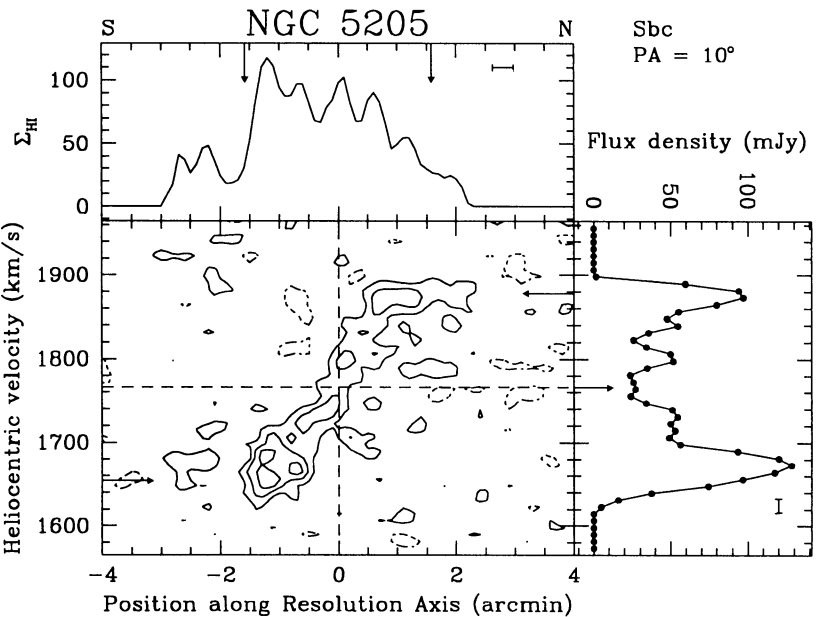
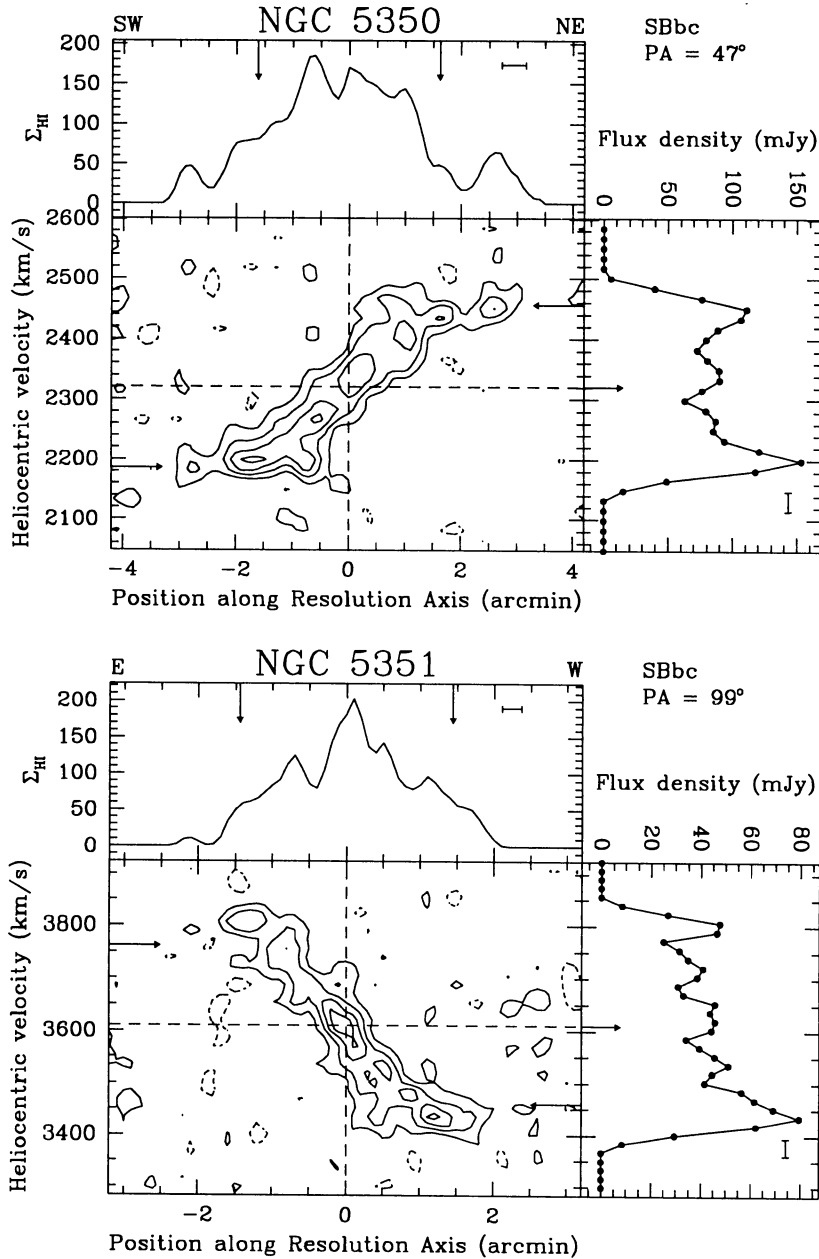
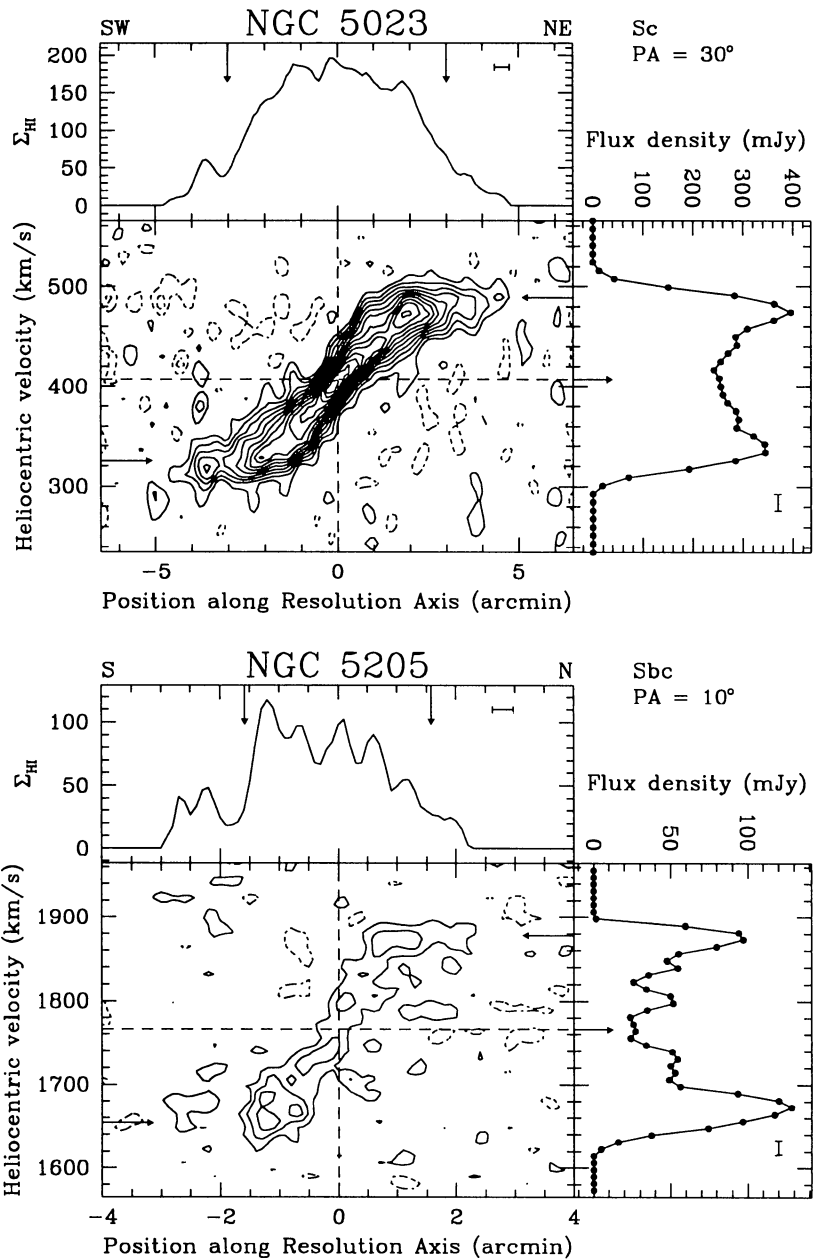


Fig. 4. continued

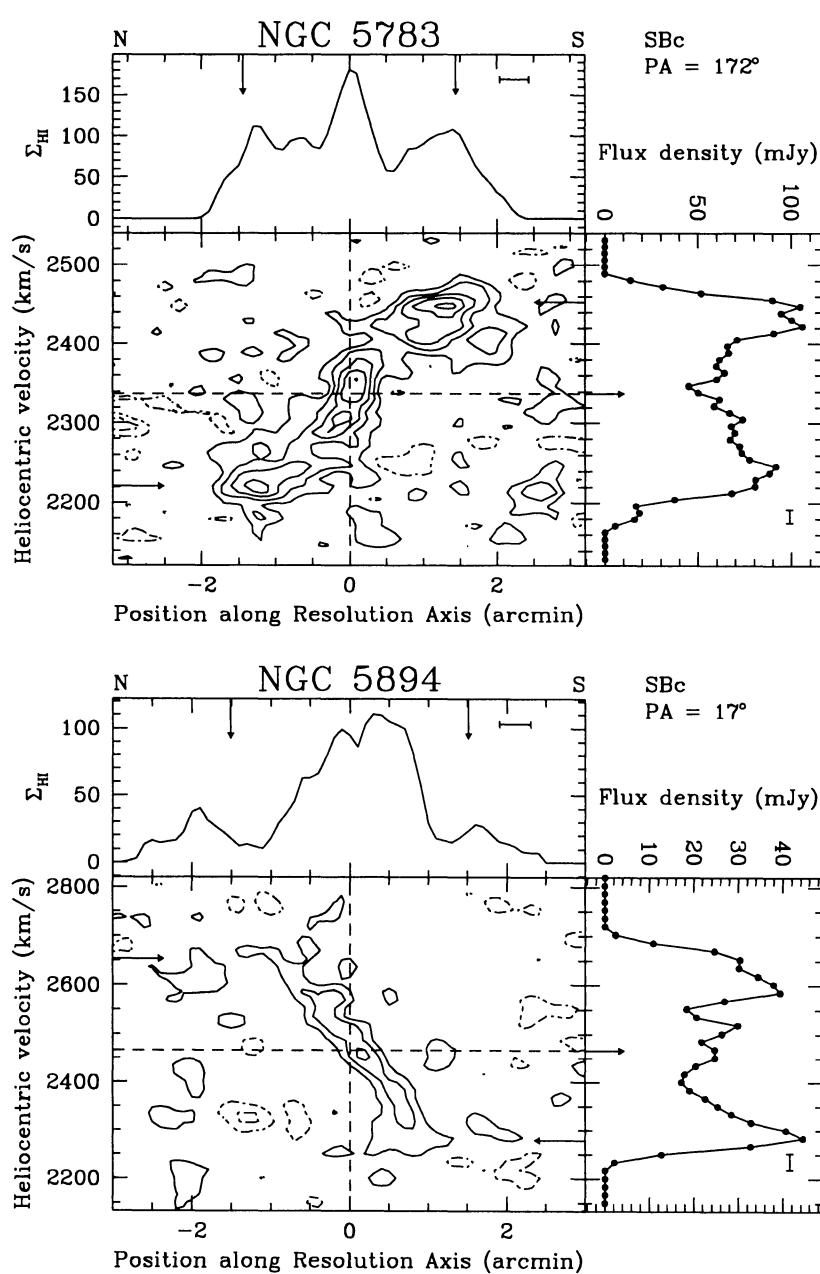
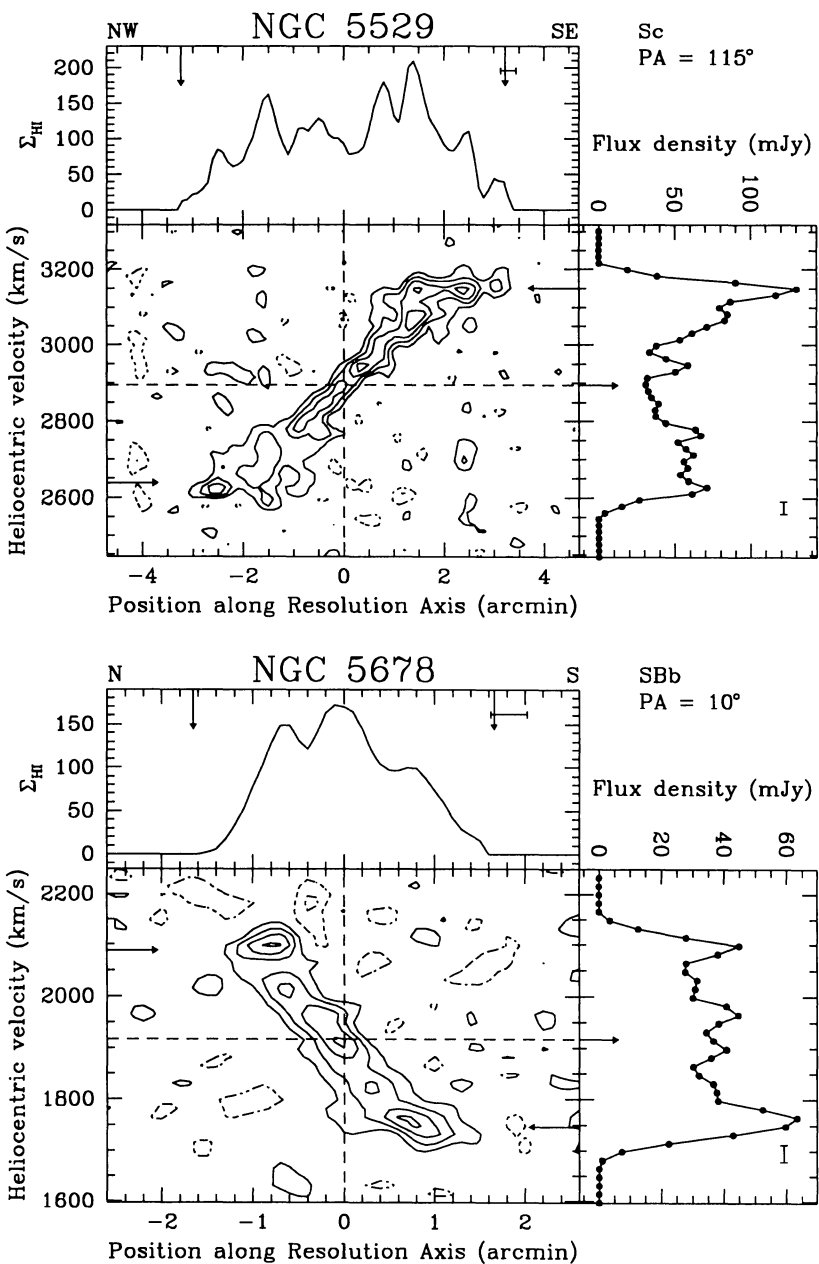


Fig. 4. continued

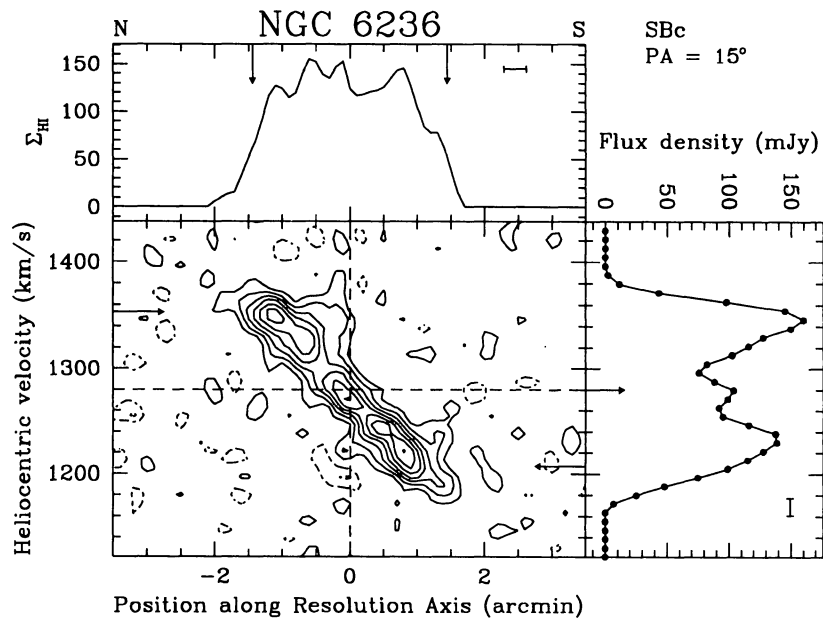
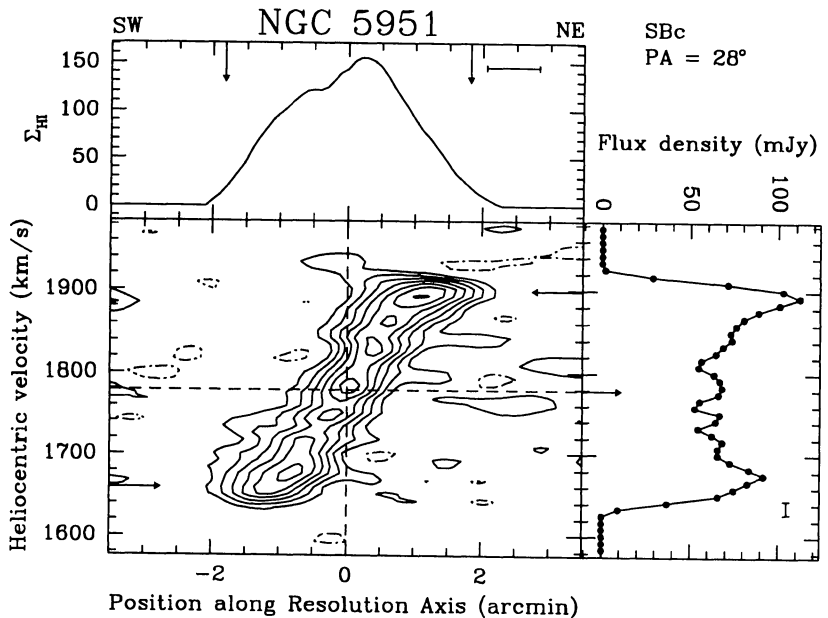
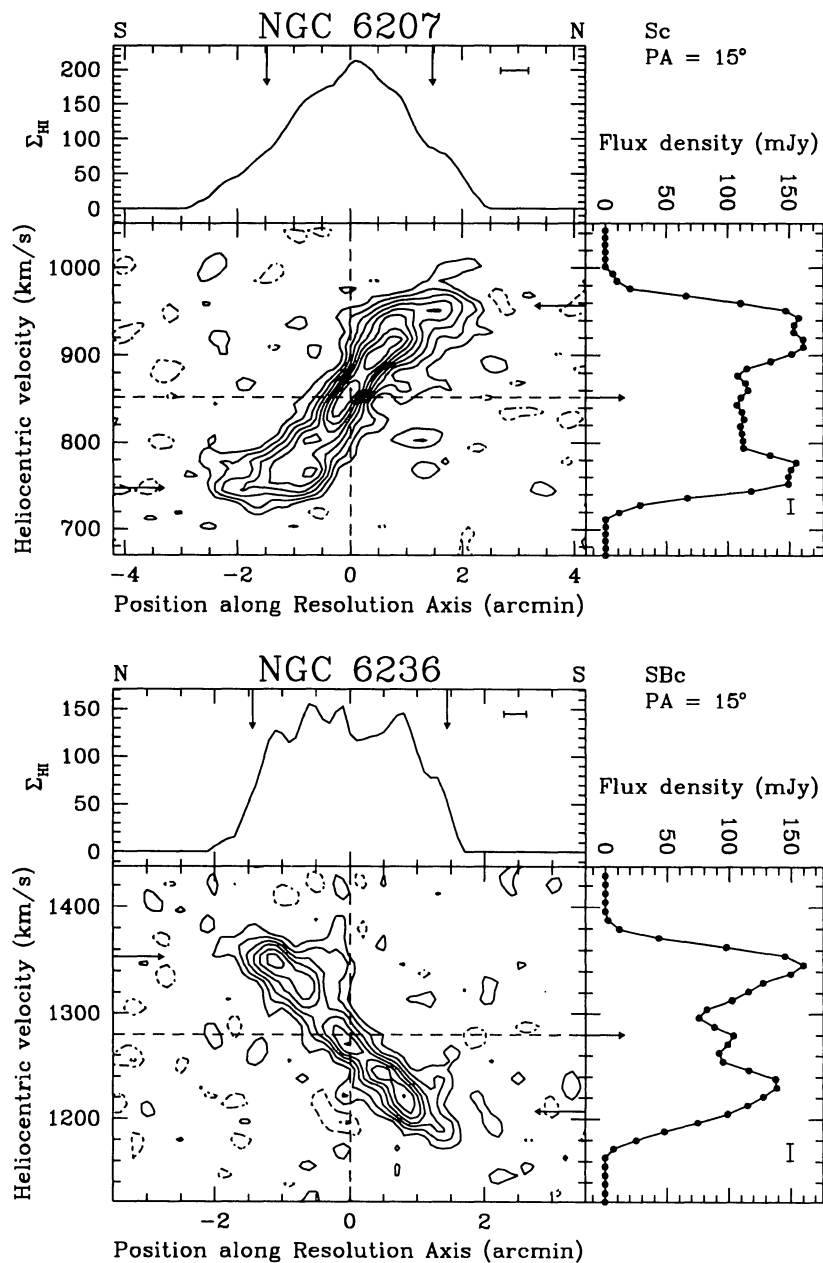
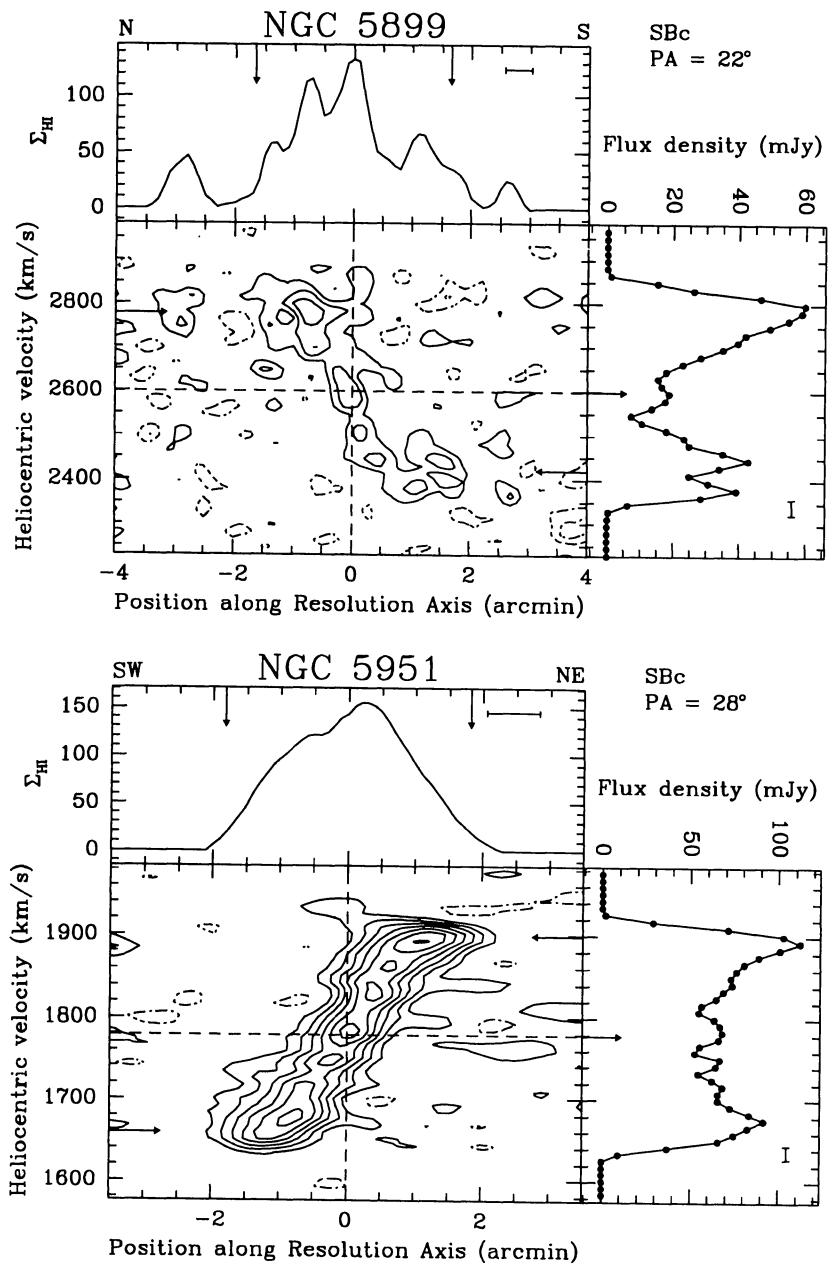


Fig. 4. continued

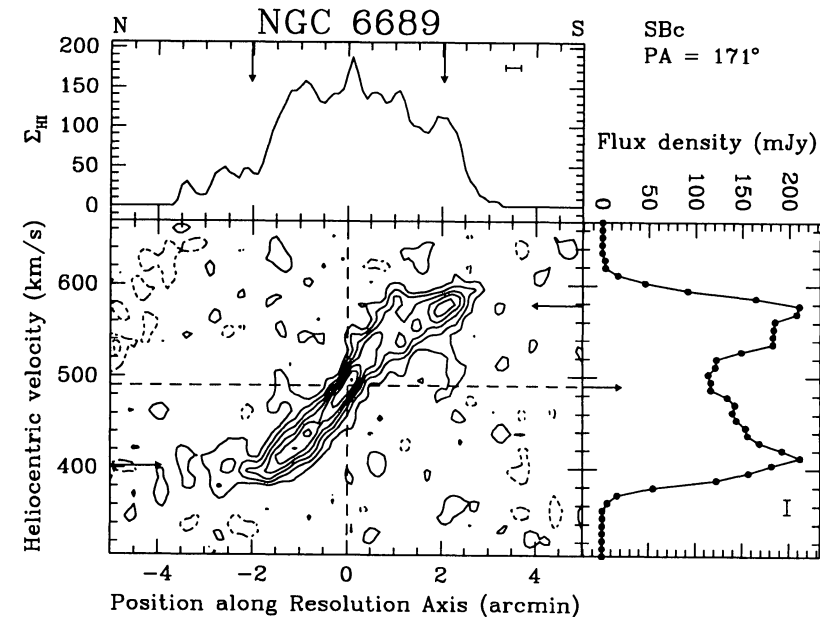
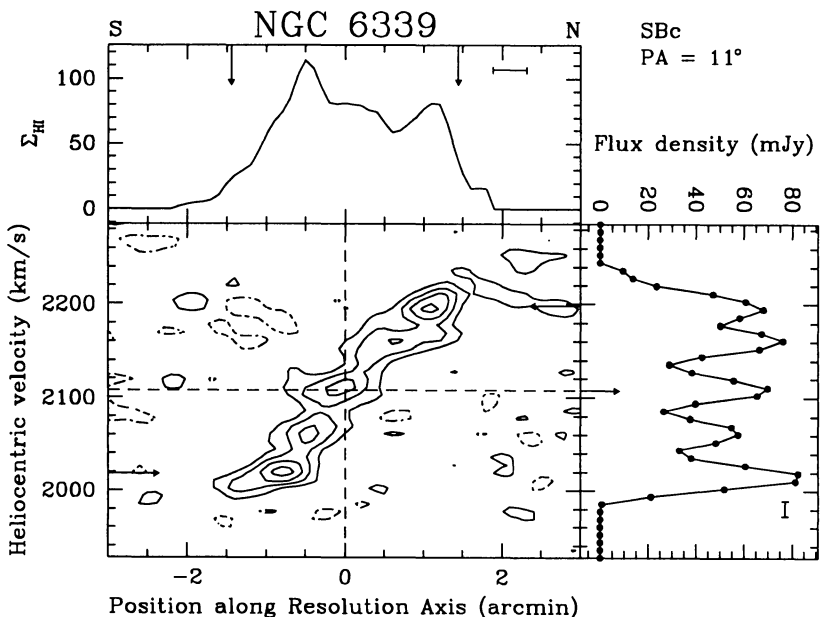
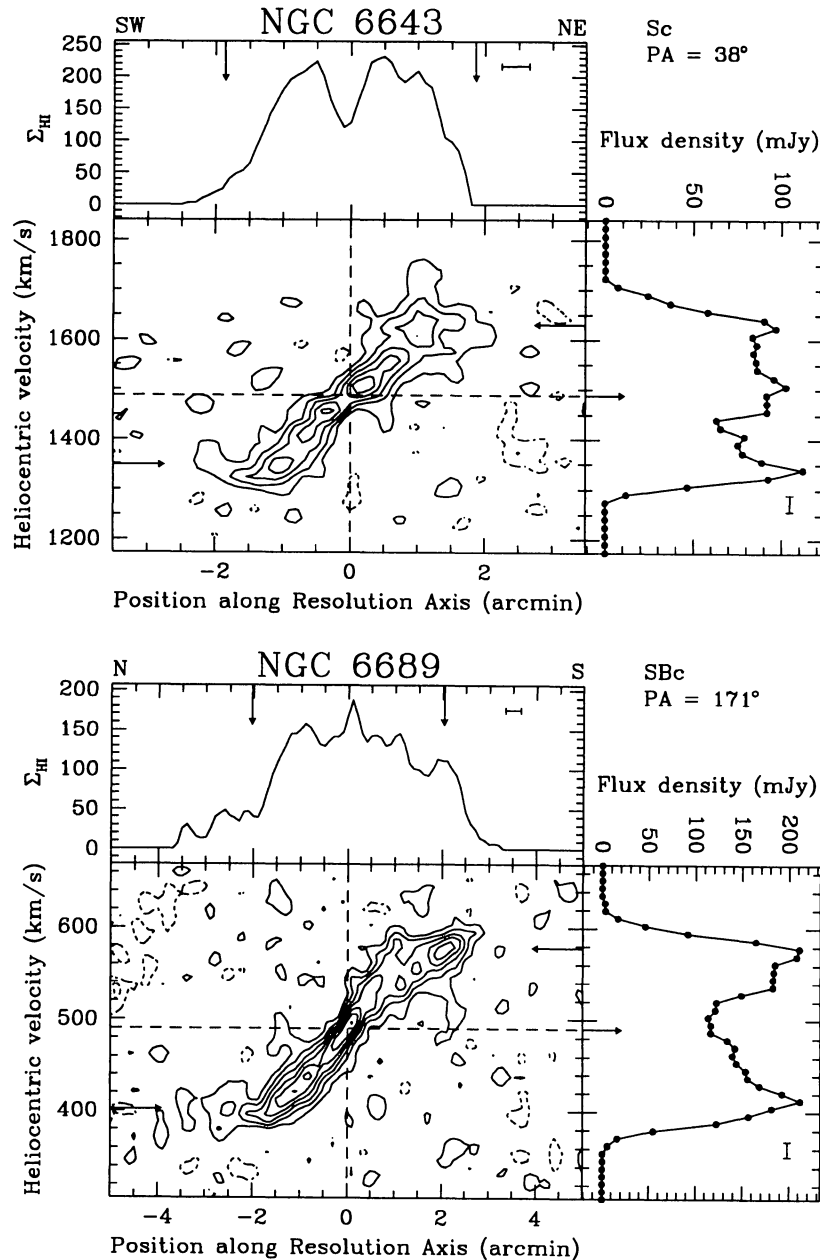
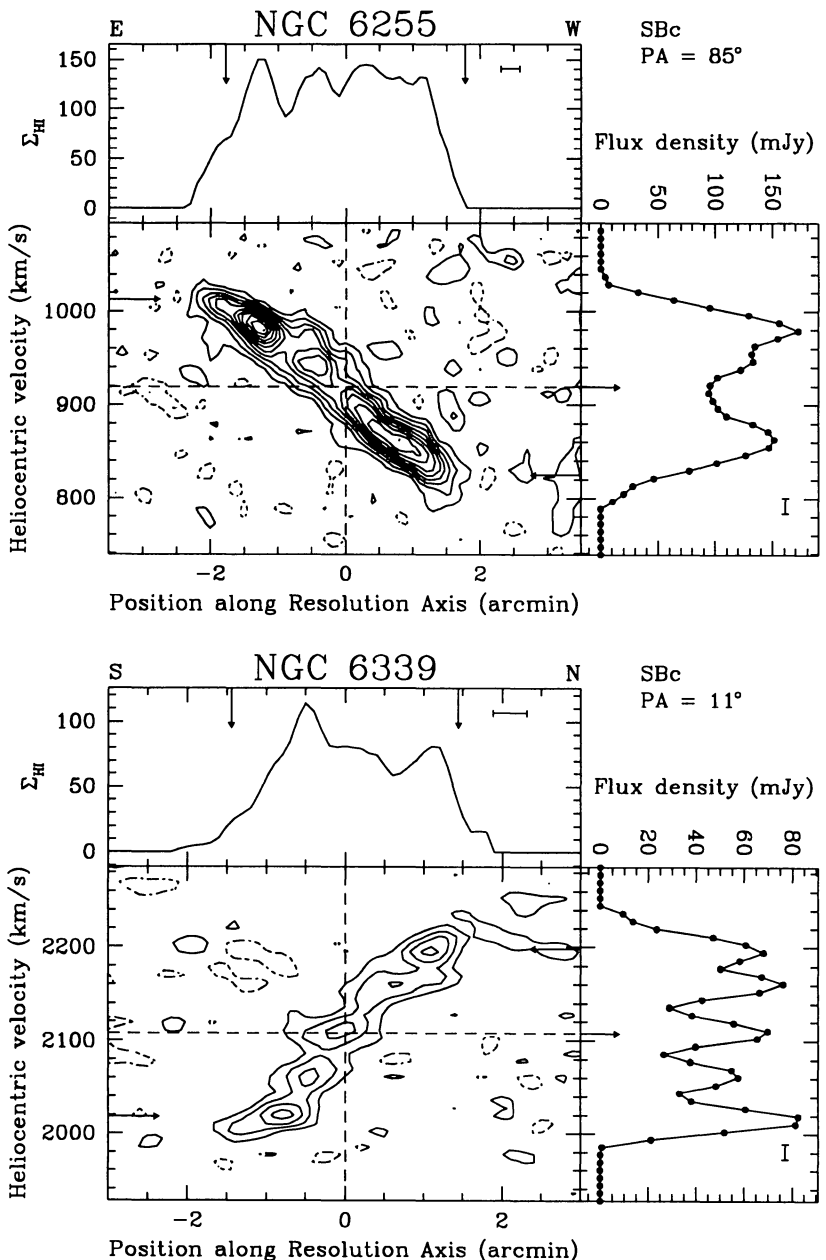


Fig. 4. continued

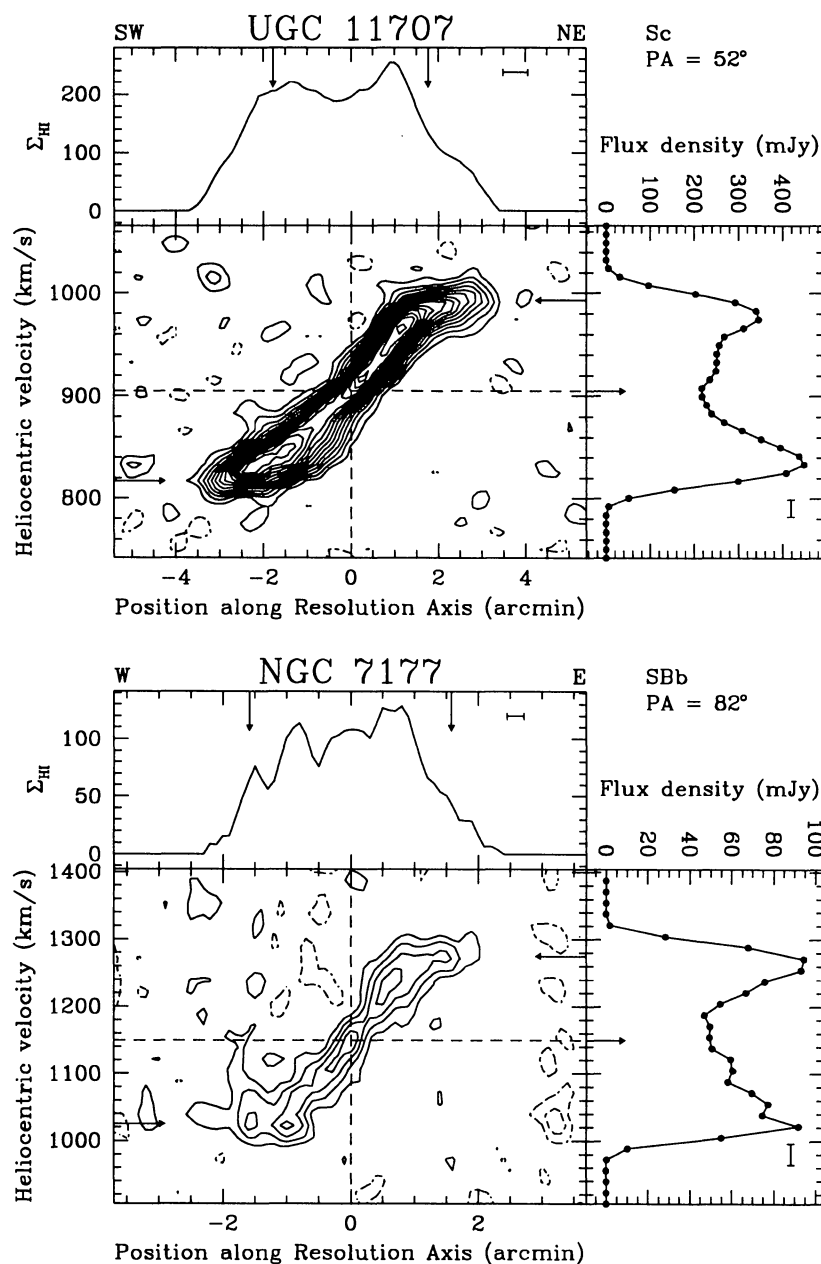
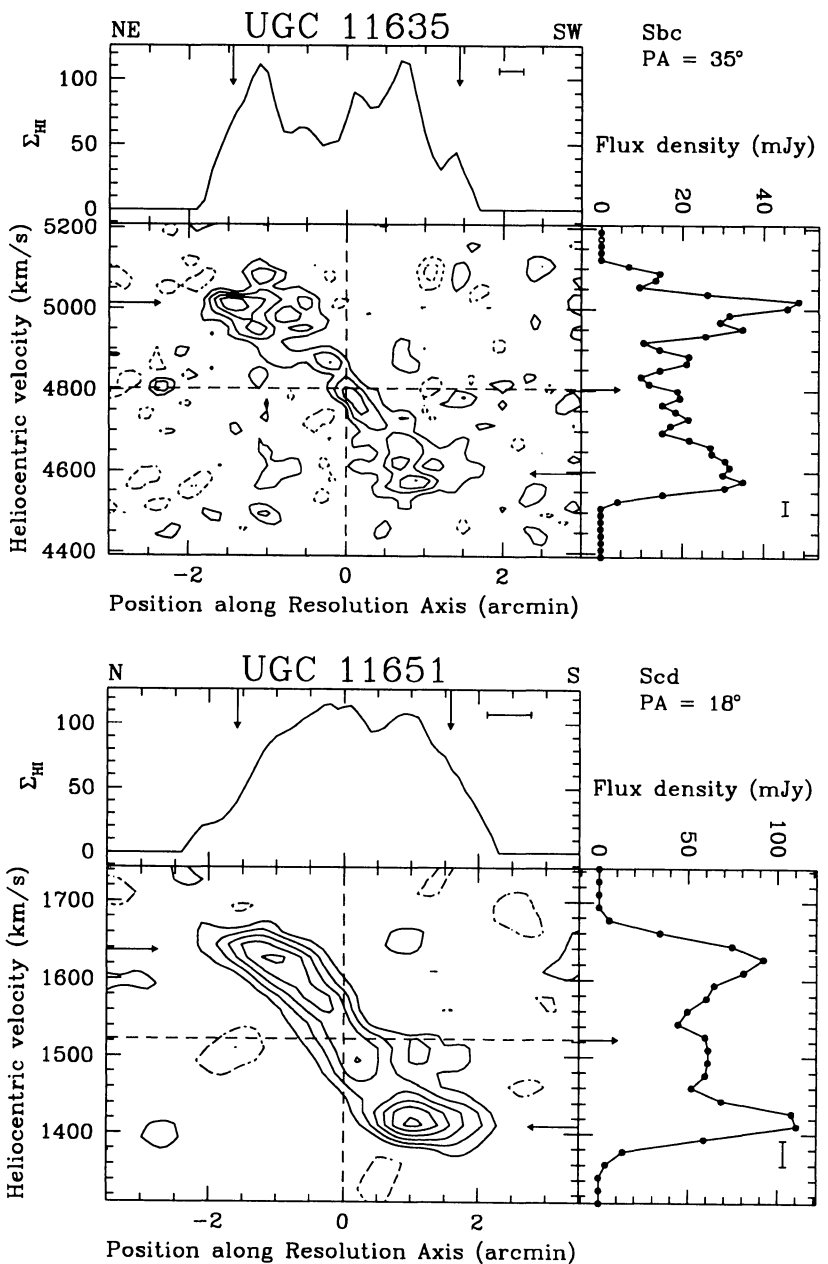


Fig. 4. continued

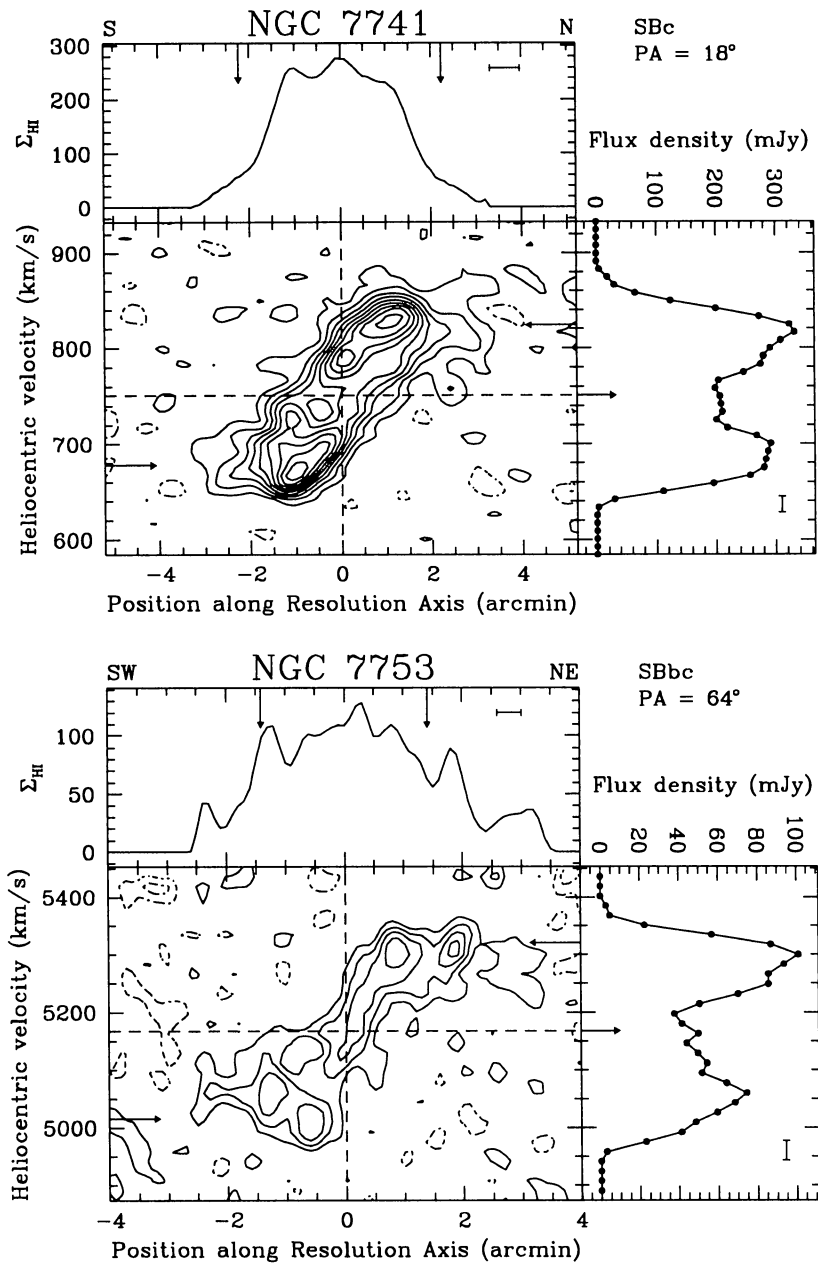
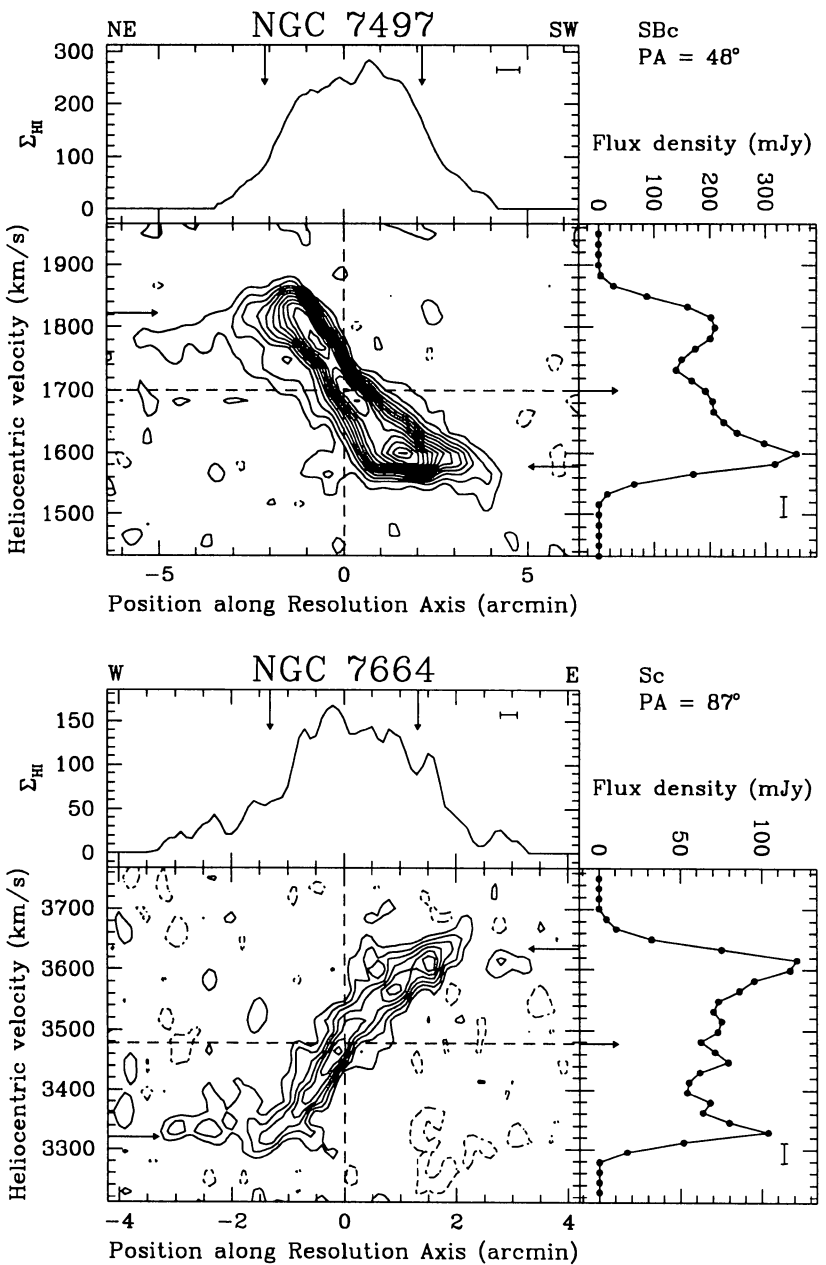


Fig. 4. continued